THESIS

LINKING FLOODPLAIN PROCESSES TO HYDROLOGIC MODELING WITH SWAT+ *GWFLOW* IN THE LOWER ARKANSAS RIVER BASIN

Submitted by

James Molloy

Department of Civil and Environmental Engineering

In partial fulfillment of requirements

For the Degree of Master of Science

Colorado State University

Fort Collins, Colorado

Summer 2025

Master's Committee:

Advisor: Ryan Bailey
Co-advisor: Ryan Morrison

Michael Ronayne

ABSTRACT

LINKING FLOODPLAIN PROCESSES TO HYDROLOGIC MODELING WITH SWAT+ *GWFLOW* IN THE LOWER ARKANSAS RIVER BASIN

Floodplain landscapes play a significant role in hydrologic fluxes, including connectivity to the alluvial aquifer and the biogeochemical processing of solutes from irrigation return flows. Variable spatial extents and limited temporal occurrence of active floodplains make quantifying their hydrologic and biogeochemical impacts problematic. To investigate, a surface-subsurface modeling practice was implemented to simulate hydrologic processes at the watershed scale in the heavily managed Lower Arkansas River Valley (LARV) (Colorado, USA). The SWAT+ model accounts for spatial variability of landscape features while simulating the fundamental physical principles that govern hydrologic processes within a watershed, such as runoff, infiltration, soil water routing, crop uptake, soil lateral flow, groundwater storage and flow, and streamflow. Using the *gwflow* module of SWAT+ simulates groundwater head, storage, and fluxes in response to hydrology and irrigation at the surface, replacing the original groundwater module. The primary objective of this thesis is to improve the implementation of floodplain landscapes in a modified version of SWAT+ with *gwflow*; and to assess the role of floodplains in aquifer recharge in the LARV. The model is run for the 1992-2020 period, with fifteen parameters calibrated for streamflow. Most years, flooding is insignificant in the managed LARV, and few floodplain-linked cells become active along the Arkansas River corridor. Flood scenarios for 100-year and 500-year events were run to observe the effects of including

floodplain-exchange in SWAT+ *gwflow* models. Water balances reveal that the hydrologic process with the largest daily groundwater flux may occur through active floodplains, with implications on the annual change in storage for an aquifer system. Groundwater contributes 13% to streamflows through the standard simulation period. During the month of a 500-year flood scenario, groundwater produced 8% of surface flows, up from 3% without integrating floodplains. Activating floodplains in the 500-year flood scenario provided an additional flux, increasing groundwater storage by 3.5 % that year. Results are largely dependent on how floodplain landscapes are delineated; findings show that incorporating floodplains and floodplain-channel interaction into models likely brings the simulation into a stronger accordance with the real stream-aquifer system, as seasonal groundwater head and fluxes (groundwater saturation excess flow, groundwater evapotranspiration, groundwater return flows) are influenced by river water seeping to the aquifer during periods of flooding. Doing so allows the LARV model, and other models that use the floodplain option, to be used for quantifying the effects of flooding events on hydrological processes, nutrient processes, and management of wetlands and cropping systems within the floodplain of a river valley.

ACKNOWLEDGEMENTS

I would like to take this opportunity to express my appreciation and gratitude to the many individuals and organizations that provided support during this project. The experience I had at Colorado State University has been very fulfilling, and I've grown significantly through my time here. Special thanks goes to my advisor, Dr. Ryan Bailey, for his continued support and patience through my research and for providing career and life guidance. The groundwater hydrology research group is a very supportive collection of researchers who provided technical assistance on many occasions and created a positive working environment. Thank you to all the graduate student peers, visiting researchers, and postdoctoral scholars I interacted with over the past two years. This Civil and Environmental Engineering degree program was very curriculum-heavy given my physical sciences background; I'm extremely grateful for Dr. Ryan Smith, Dr. Michael Ronayne, Dr. Joseph Scalia, Dr. Christopher Bareither, Dr. Lisa Stright, Dr. Jeffery Nieman, and Dr. Ryan Morrison for providing support, engaging curricula, and fostering excitement for research and engineering in water and natural resources.

Many individuals in my life played a role in this success beyond campus. Family and friends provided love, support, and balance through my graduate efforts. Former coworkers at Nelson Engineering backed my efforts to seek higher education and instigated me to pursue a career in for groundwater hydrology. Advisors from my undergraduate research Dr. Donald Rodbell and Dr. David Gillikin provided my first incredible research opportunity that ultimately brought me here today.

Acknowledgement and gratitude for the funding sources that contributed to my graduate achievements go to the Colorado State University Agriculture Experiment Station, the Tipton & Kalmbach/Stantec Graduate Fellowship, and the Whitney Borland Scholarship.

The success of this project is made possible by the contributions and support of the people who surround me. I consider myself extremely fortunate to be in this position, and I'm forever grateful to my peers, faculty, friends, and loved ones.

TABLE OF CONTENTS

LIST OF TABLES

LIST OF FIGURES

LIST OF EQUATIONS

1. INTRODUCTION

1.1 Floodplain Interactions

Discharges of flood-stage flows route through channel networks in a brief temporal event, unlike many continuous hydrologic and biogeochemical processes (Junk et al. 1989). Floodplain-linked batch processes only activate where and when overbank flows occur. Spatial and temporal occurrence of flooding is controlled by conditions such as river stage and soil moisture (Saskena et al. 2017; Wasko and Nathan 2019), and morphology of the channel and alluvial plain (Wohl 2021). Beyond peak discharge rates, variations in floodplain storage volumes are a result of spatial heterogeneity of the landscape (Wohl 2021) Tull and Passalacqua 2025), while flood stage resonance times and attenuation are greatly influenced by conveyance over the floodplain and by secondary channels (Tull and Passalacqua 2025). Field observations and integrated flood inundation models have shown that greater extents of soil saturation before a flooding event increases the total area inundated (Saskena et al. 2017).

Floodplain landscapes act as an interface between river channel networks and groundwater systems for the exchange of water and solutes. Complex and dynamic processes such as bank storage, overbank inundation, recharge, pumping, evapotranspiration, and saturated zone exchange (Jolly and Rassam 2009) must be considered in the floodplain subcategory of groundwater-surface water interactions in semiarid regions. Modeling approaches that include groundwater and unsaturated zone exchange greatly improve the accuracy of flood predictions (Wasko and Nathan 2019). Bates et al. (2000) deployed a grid of piezometers to compare with a hydrogeologic numerical model to observe groundwater processes during an overbank event. Findings from numerical simulations compared with floodplain piezometer indicate that that floodplain soils became near-saturated in the upper 5 m, and that floodplain exchange with

streams occurs in a near-saturated condition (Bates et al. 2000; Kollet and Maxwell 2006). Following a flood event, recharge induces groundwater ridging, affecting groundwater head distributions. Most groundwater follows a 2-D lateral flow toward hillslopes outside the initial and final stages of an overbank event (Bates et al. 2000).

Floodplains serve important ecological functions and are among the most threatened ecosystems; watersheds that receive annual and low return period events develop a diverse variety of habitat structures and have improved water quality (Opperman et al. 2010). Floodplain-aquifer exchange occurs infrequently, but the connection is adjacent to the hyporheic zone with dynamic biogeochemical activity (Harvey and Wagner 2000). In addition, overbank inundation may reduce accumulations of salts from plant-root zones where groundwater is shallow (Wolski et al. 2006).

A previous SWAT+ modeling investigation by Bieger et al. (2019) showed that the ratio of upland to floodplain landscape areas has minor implications on streamflow. However, floodplain connectivity increased groundwater contributions to streamflow while reducing surface runoff's contribution to the hydrograph. Further developments in SWAT+ modeling framework to include surface hydrologic connections floodplain landscapes improve streamflow performance at both base and peak discharges (Wagner et. al 2019).

A SWAT+ *gwflow* (Bailey et al. 2023) model of the upper Colorado River that includes landscapes identified that floodplain exchange with the aquifer reduces surface runoff and soil lateral flow while increasing saturation excess flow and total recharge (Schultz et al. 2024). Landscape hydrological-groundwater numerical models that include floodplain-aquifer exchange remain largely uninvestigated, particularly in irrigated regions.

1.2 Process-Based Modeling of Managed Watersheds

Water management issues such as soil salinity, waterlogging, canal seepage, and interstate compacts are complicated but common issues in regions with established irrigation industries (Gates et al. 2006). Aquifer-stream connections in irrigated alluvial valleys present many complicated and competing processes, presenting the need for integrated modelling approaches (Navas et al. 2025). Estimating the full water budgets for evapotranspiration, streamflows, and groundwater in tandem constrains hydrologic fluxes to realistic ranges (Abbas et al. 2025). Excess irrigation discharges may provide delayed recharge through winter months, supplying baseflows to rivers with implications at the field scale (Kendy and Bredehoeft 2006).

To capture the numerous processes occurring on the surface, the SWAT+ model discretizes the landscape into hydrologic response units with unique combinations of properties governing the mass balance of water, nutrients, and sediment at a field-scale resolution (White et al. 2022). SWAT+ interacts with groundwater through the *gwflow* module subroutine, which is a physically based, fully distributed numerical groundwater model to simulate the conservation of mass across unit volume boundaries, through zones with variable aquifer properties, and the numerous physical processes that exchange water with the saturated zone (Bailey et al. 2023). Within the SWAT+ modeling code, the *gwflow* module is called as a subroutine, replacing the original groundwater module. Figure 1 shows the hydrological processes simulated by the SWAT+ model, with the *gwflow* module active.

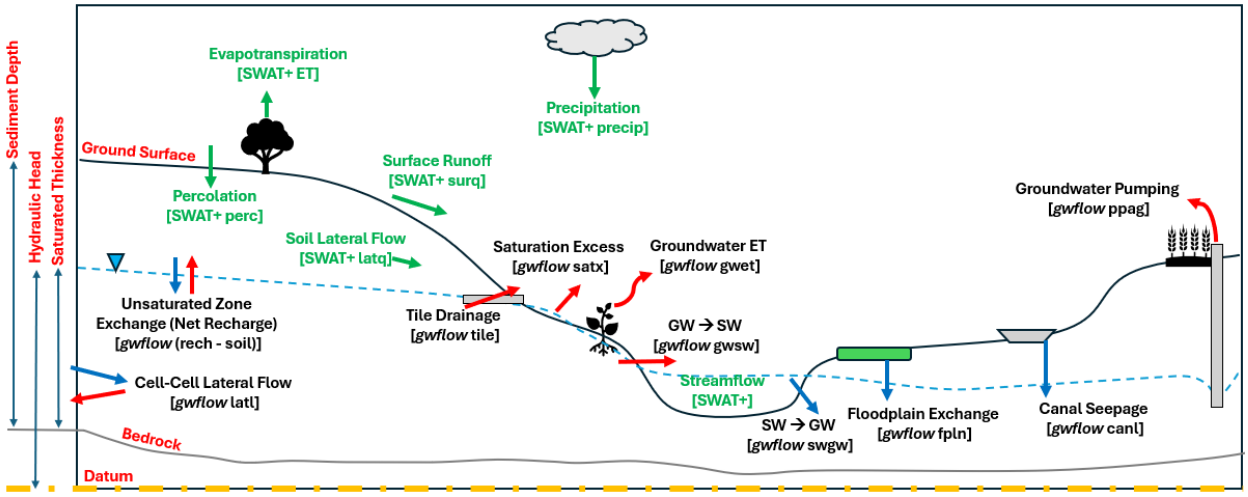

Figure 1: Schematic showing active processes modeled with the SWAT+ *gwflow* hydrologic mass balance. SWAT+ processes are labeled with green text; *gwflow* processes are labeled with black text; surfaces and important dimensions are labeled with red text. *Gwflow* processes that remove groundwater have red arrows, while processes that add groundwater have blue arrows.

1.3 Research Objectives

The Lower Arkansas River Valley (LARV) is a highly managed watershed in southeastern, Colorado. Challenges with soil salinity and high water tables and soil salinity has presented challenges for LARV users and the need for decision making tools such as integrated watershed models. Existing LARV models constructed with MODFLOW-NWT (Morway et al. 2013), SWAT-MODFLOW (Bailey et al. 2013), and SWAT+ *gwflow* (Abbas et al. 2024) highlight the importance of certain processes, provide a guideline for parameter values, and estimate the magnitude of water budget components.

This study aims to independently create and calibrate an integrated watershed and groundwater model with SWAT+-*gwflow* for the Lower Arkansas River Valley to investigate the role of floodplains in their contribution to groundwater recharge and baseflow contributions, as well as the spatial and temporal significance of floodplain landscapes in groundwater-stream

exchange. The integration of floodplain exchange may influence the discharges to and from groundwater by other processes. A full assessment of how SWAT+ *gwflow* modeling with floodplains changes water balance components surrounding overbank events. The outcomes of this research will assist scientists and managers in understanding the role of floodplain landscapes in agriculturally dominated river systems.

2. METHODS

2.1 Study Region

The Arkansas River originates in central Colorado's Sawatch Range and flows East across the western Great Plains before crossing into Kansas. The area of interest (Figure 2) is located between Pueblo Reservoir and the town of Las Animas, upstream of Jon Martin Reservoir. Located in the eastern plains of Colorado, the study area has a cold semi-arid climate receiving 150 to 560 mm of precipitation a year (Gates et al. 2012). The Fryingpan-Arkansas Project delivered water from west of the continental divide to Pueblo Reservoir (Gates et al. 2012). The Lower Arkansas River is connected to an alluvial aquifer and crosscut with canals supplying irrigation for the region's steadfast agriculture industry (Gates et al. 2006). Crops grown include hay, corn, grains, and sorghum grass (USDA 2019). High water tables from decades of intense irrigation have created issues with soil salinity, waterlogging, reduced crop yield, and mineral pollutant issues (Gates et al. 2012; Gates et al. 2006; Triana et al. 2009).

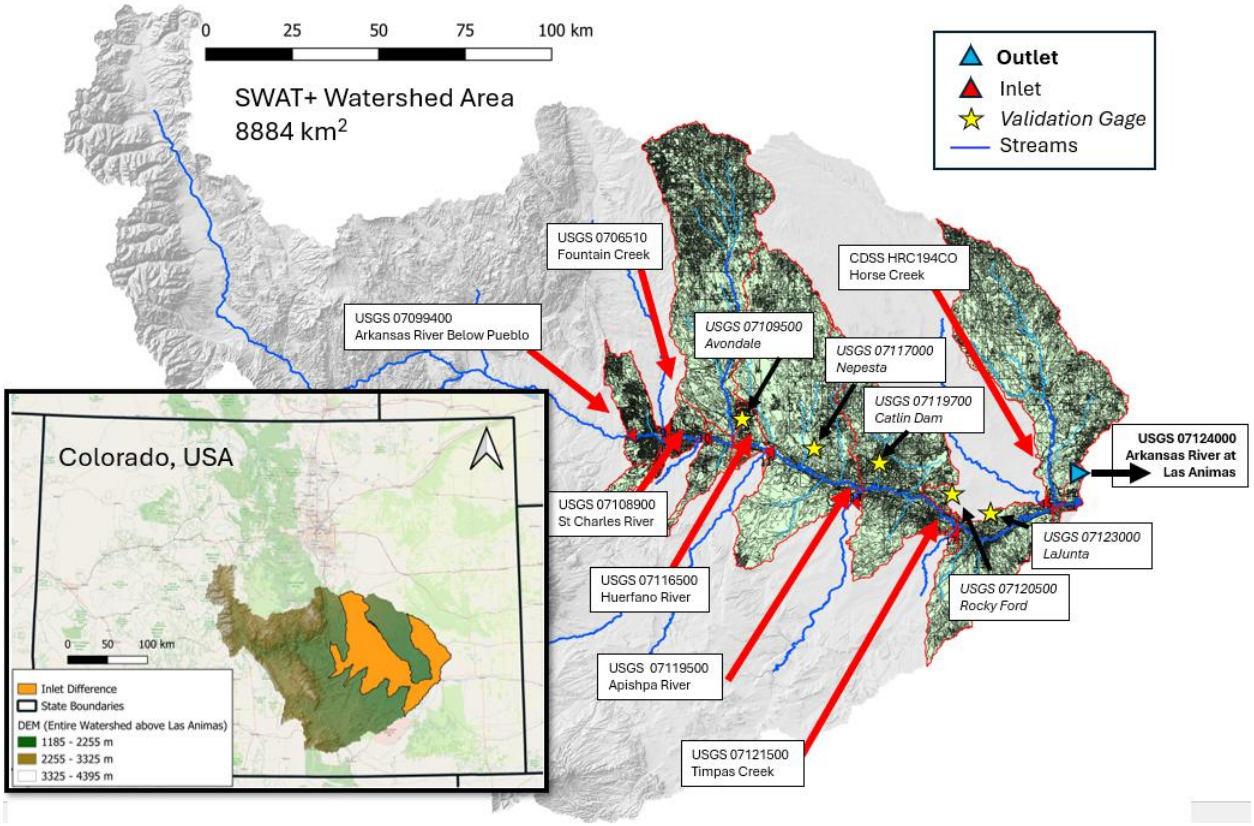

Figure 2: Map showing the entire Arkansas River Basin above the model outlet stream gauge in Las Animas, and the model's spatial extent clipped from drainage areas upstream of Inlet point sources. Stream gauges used for model calibration are labeled with stars and callouts with black arrows.

2.2 Models and Model Setup

The LARV was modeled using the SWAT+ model (Bieger et al. 2017) to capture hydrologic processes in soil and the surface, with the spatially distributed *gwflow* module (Bailey et al. 2020; Bailey et al 2023) to model hydrologic solute mass balance processes in the saturated zone. Additional model setup included creating *gwflow* package input files to include canal seepage, tile drainage, and floodplain recharge. In addition, diversion data and a water allocation file were prepared to assign irrigated fields to their irrigation practice and sources. The workflow in Figure 3 summarizes the input data and routines used for model setup. More information regarding input data and input files are provided in the following sections.

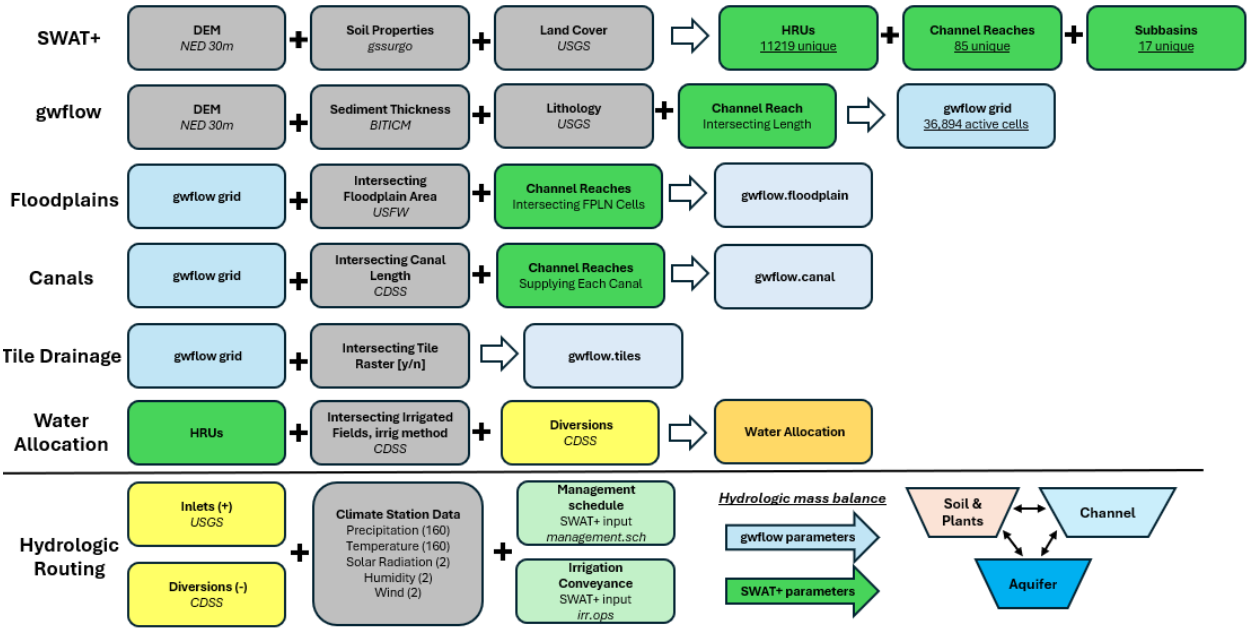

Figure 3: Diagram summarizing the model development workflow. Grey sections indicate geospatial data, green for SWAT+ inputs, blue for *gwflow* files, yellow for point sources, and orange for water allocation.

2.2.1 SWAT+ setup

Initializing SWAT+ input files included working with large spatial datasets. The QSWAT module for QGIS was utilized to process spatial data with the SWAT+ Editor to create input files (Molina-Navarro et al. 2018). QSWAT routines computed flow directions, extracted the stream network, and delineated the watershed above the chosen outlet station in Las Animas, CO from a 30 m DEM from the National Elevation Dataset (Gesch et al. 2018). Next, the locations of USGS gaging stations were selected as inlet point sources and clipped the upstream tributary's watershed area. From this stage, QSWAT discretized 85 channel reaches and 17 subbasins.

Soil properties from the gridded Soil Survey Geographic Database, gSSURGO (Soil Survey Staff, 2023), and the National Land Cover Database (Dewitz, 2021) were added in the later steps of the QSWAT procedure to identify unique combinations of soil properties, land

cover, and topography to create hydrologic response units and landscape units. QSWAT geospatial outputs are opened in the SWAT+ editor to create input files for the model.

2.2.2 *GWFLOW* setup

Darcy's law and the specific storage are the fundamental governing conservation of mass equations used by the *gwflow* subroutine for SWAT+ for transient simulation groundwater storage, groundwater head, and groundwater flow within the unconfined aquifer of the LARV. A control volume approach calculates hydraulic head and storage using the previous time step's head values from surrounding cells with, and fluxes from process-based interactions with other cells and the surface (Bailey et al. 2020). Equation 1 shows components of the groundwater balance calculated by *gwflow* with term descriptions provided in Table 1. Net recharge will consolidate soil transfer and deep percolation processes, and groundwater-surface water exchange will be consolidated by the sum both unidirectional processes.

$$\Delta S = [\text{Net\_rech}]_1 + [\text{swgw} - \text{gwsw}]_2 - \text{gwet} - \text{satx} - \text{ppag} - \text{tile} + \text{canl} + \boldsymbol{fpln} +/- \text{latl}_x +/- \text{latl}_y \quad (1)$$

Table 1: Components of the *gwflow* balance

Q component (m^3/day)	Description	Calculated with:	
Net_rech_1	soil water added to groundwater - groundwater transferred to HRU profile	NA	SWAT+ HRUs
gwet	groundwater removed by evapotranspiration	Head	Linear Eqn
gwsw_2	groundwater exchange with streams	Head	Darcy's Law
satx	saturation excess flow (water table above ground)	Head	Darcy's Law
latl	groundwater transferred between cells	Head, Specific Storage	Darcy's Law
ppag	groundwater pumped for irrigation	Specific Storage	Storage Eqn
tile	groundwater removed via tile drains	Head, Specific Storage	Darcy's Law
canl	canal seepage to groundwater	Head	Darcy's Law
fpln	floodplain exchange	Head	Darcy's Law

The workflow in Figure 3 identifies the geospatial input data and processing steps required to create *gwflow* input files using the original SWAT+ shapefiles, the 30 m DEM, the State Geologic Map Compilation of USGS surface lithology data (Horton et al. 2017), and the SoilGrids250m2017-3 gridded dataset for sediment depth to bedrock (Shangguan et al. 2017). Creation of *gwflow* files was automated using the fortran code modified from Bailey et al. (2023). The *gwflow* setup follows:

1. Creating the *gwflow* grid over the watershed extent (308 rows and 315 columns). A 500m grid was chosen for this study.
2. Intersecting the watershed boundary to flag cells as active, inactive, or boundary (36,894 active and inactive cells). A no-flow boundary condition was selected, due to the long distance between the boundary and the alluvial aquifer.
3. Extracting and assigning cell ground surface elevations and unconsolidated sediment thickness.
4. Joining surface geological data to assign geologic properties (seven zones for hydraulic conductivity and specific yield). Zones of surface lithologies are mapped in Figure 4.
5. Intersecting channel reaches for river cell elevation, cell-channel length, channel reach ID (for river stage), and assigning depth to channel below DEM, streambed hydraulic conductivity, and bed thickness.
6. Intersecting the HRU shapefile with the *gwflow* grid.

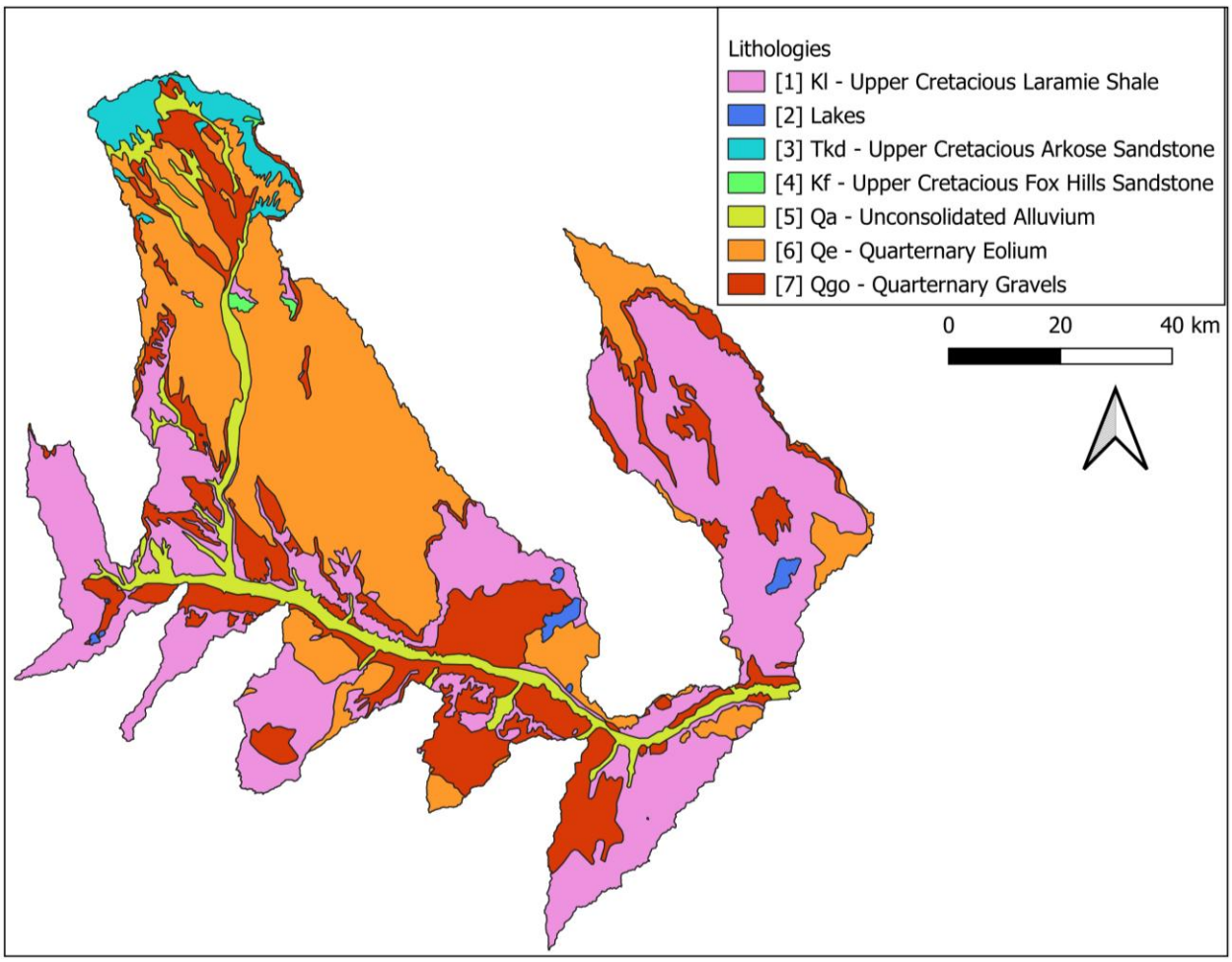

Figure 4: Surface lithologies (Horton 2017) within the model extent used to assign zones for aquifer properties.

The *gwflow* subroutine calculates groundwater head and fluxes on a daily timestep, without the option for steady-state computation. Input data was prepared for all inlets from 1992 through 2020 and the model was run in transient simulation through that entire period. To implement a spin-up period for head calculations to equalize, the first six years of output data (1992-1997) were not considered with other results.

2.2.3 Irrigation and Water Allocation

A water allocation file was prepared to connect irrigated lands with their method and source of irrigation. SWAT+ procedures created a unique HRU for each irrigated parcel for accurate assignment in water allocation. The HRU shapefile was intersected with the Colorado Decision Support System's Division 2 (https://cdss.colorado.gov/gid-data/division-2-arkansas) Irrigated Fields data (Figure 5) to add HRU attributes of irrigation data. Irrigation methods were designated between flood and sprinkler irrigation for all HRUs, several fields used drip irrigation but were modified to be read for sprinkler irrigation methods by SWAT+ for simplicity. Application efficiencies of 0.85 for sprinkler and 0.7 for flood irrigation are appropriate for the region and kept in the *irr.ops* decision table (Gates et. al 2006).

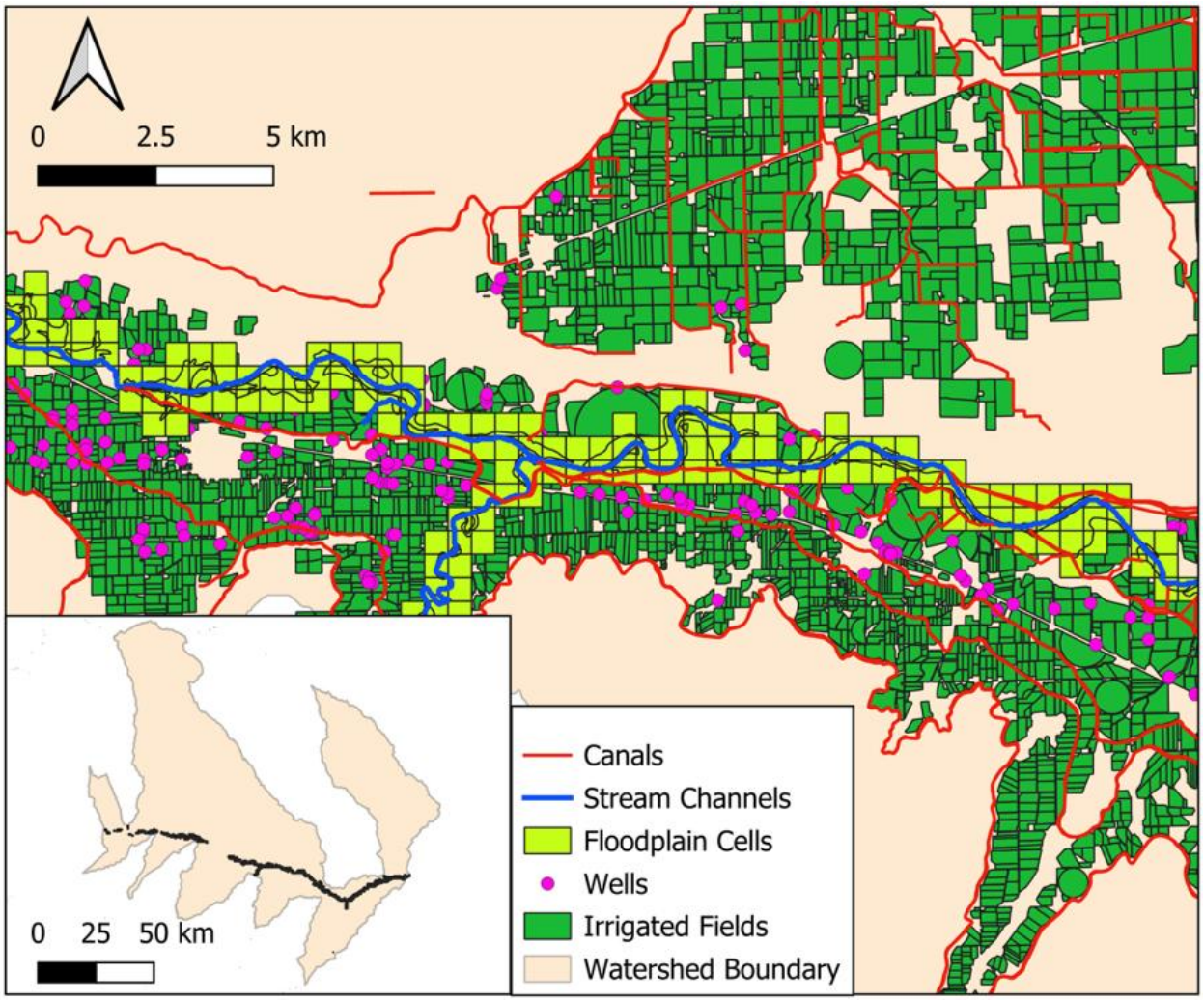

Figure 5: Map of the LARV with canals, wells, and irrigated fields illustrate the complexity of water allocation. Riparian areas delineated for floodplains is shown.

Fields may be irrigated from a single or multiple sources. Well-supplied irrigation connects the HRU with water from the intersecting *gwflow* cell; fields supplied by a canal are connected to diversion files. Diversion files act as point diversions along channel reaches containing daily withdrawals from all canals along a SWAT+ channel. A conceptual model of inlet confluences and diversion locations along the mainstem Arkansas River is provided in Figure 6.

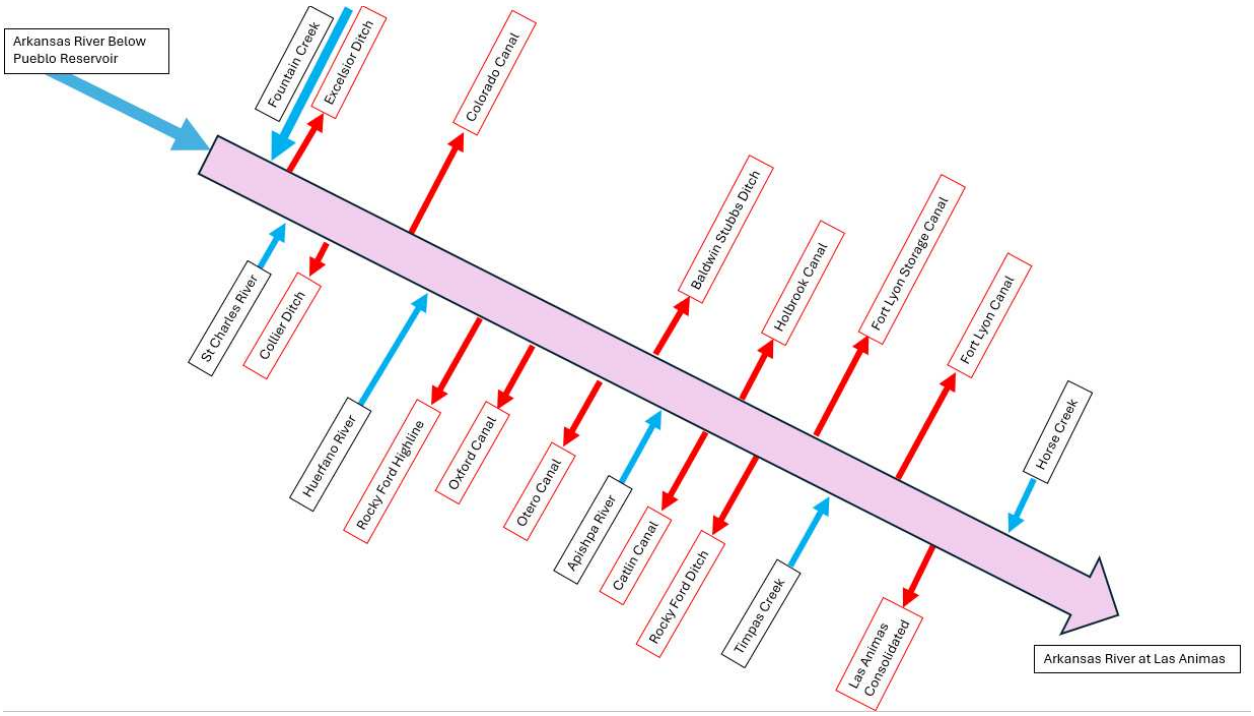

Figure 6: Conceptual model showing the inlets and diversions that add and remove flows along the Lower Arkansas River's channel from the inlet below Pueblo Reservoir to the model outlet at Las Animas.

2.2.4 Canal Seepage

Canal seepage was introduced by a flag in the *gwflow* subroutine to read the *gwflow.canals* file. Data includes a list of all canal-connected *gwflow* cell IDs, a reference to the SWAT+ point source diversion, canal length across the *gwflow* cell, and canal hydraulic conductivity zones (see notes in section 2.3). Canal width was measured mid-profile from satellite imagery and canal depth was set to 0.25 m. Canals operate from April 1st through October 15th with a canal stage for each cell set 1 m below the DEM ground surface. Canal seepage cell discharges and fluxes (canl) are calculated using Darcy's Law (Equation 2) with the cell's canal width (w), length (l), canal hydraulic conductivity (K_{canal}) across the canal bed thickness (bedthick), and head difference between the canal stage and aquifer (ΔH) as described in Equation 1 (Almahawis et al. 2024). The *gwflow* canal seepage program assumes a saturated condition below canals.

$$canl = (w*l)*K_{canal}*(\Delta H/bedthick) \quad (2)$$

2.2.5 Tile Drainage

Tile drainage was incorporated into the groundwater model by intersecting the national tile drainage raster dataset presented by Valayamkunnath et al. (2020) with the *gwflow* grid. Tile drainage is not expected to be widely used throughout the LARV, so the density of tile drain *gwflow* cells was reduced by a factor of ½. Discharge to the surface by tile drainage is calculated with Darcy's law (Equation 3) when head exceeds drain elevations using hydraulic conductivity and exterior surface area of drains (Bailey et al. 2022).

$$tile = K_{tile}*A_{drain}*(h-z_{drain}) \quad (3)$$

2.2.6 Floodplain Exchange

Delineation of floodplain landscapes for *gwflow* was achieved by intersecting the shapefile for riparian habitat from the U.S. Fish and Wildlife Service retrieved July 24, 2024 from http://fws.gov/program/national-wetlands-inventory/wetlands-mapper to summarize the floodplain area over *gwflow* cells and connected SWAT+ channel reach. Discharge to groundwater from floodplains occurs when SWAT+ channel reaches simulate overbank flow conditions; flow is described by Darcy's Law in Equation 4 with floodplain hydraulic conductivity, floodplain area, and difference of connected channel stage (S_{riv}) and cell hydraulic head. Conversely, discharge is routed to the connected channel reach when hydraulic heads exceed floodplain cell DEM ground surface elevations. This feature of *gwflow* was first introduced in the work of Schultz et la. (2024) in the Colorado River Basin, for natural hydrologic conditions.

$$fpln = K_{fpln}*A_{fpln}*(S_{riv}-h) \quad (4)$$

Floodplain landscapes are geomorphic structures in fluvial systems that are periodically inundated (Wohl 2021). This study used a shapefile of riparian habitat areas for floodplain delineation. Through the remainder of the study, "riparian" only refers to the method of floodplain delineation for model setup. Land area subject to inundation during bankfull events is the primary interest to this study.

2.3 Parameters and Calibration

Parameters used within SWAT+ and *gwflow* are process-based and must be held within a realistic range for calibration (Arnold et al. 2012). Parameter value iterations were automated using the PEST batch-style programs for sensitivity analysis and calibration with monthly average streamflow rates at the model outlet in Las Animas as the calibration target. Parameters for calibration were selected by identifying those with the highest average sensitivity for May and June when highest streamflow events typically occur. A total of 86 parameters are included (Table 2), from 11 input files. The definition of each parameter is included in Appendix A. PEST calibration identifies optimal parameter values by nonlinear least squares regression for tested values (Doherty 2010); calibrated parameter values are provided in Table 2.

Table 2: All parameters considered for uncertainty analysis with initial values and testing ranges grouped by their corresponding input files. Parameters selected for calibration are in bold with their calibrated value.

Input File	Parameter	Units	Initial Value	Minimum Value	Maximum Value	Calibrated Value
cntable.lum	rcstrogcna		60	55	66	
	rcstrogcnb		72	67	76	
	rcstrogcnc		**80**	**77**	**82**	**80**
	rcstrogcnd		**84**	**83**	**86**	**84**
	brush_fcna		35	31	44	
	brush_fcnb		56	45	62	
	brush_fcnc		70	63	73	
	brush_fcnd		**77**	**74**	**81**	**77**
	pastg_fcna		49	42	58	

	pastg_fcnb		69	59	74	
	pastg_fcnc		**79**	**75**	**81**	**79**
	pastg_fcnd		**84**	**82**	**87**	**84**
hydrology.hyd	esco		0.95	0.1	1	
	epco		0.5	0.1	1	
	perco		**0.9**	**0.1**	**1**	**1**
gwflow.input	rech_del1	days	3	1	50	
	rech_del2	days	3	1	50	
	rech_del3	days	3	1	50	
	rech_del4	days	3	1	50	
	rech_del5	days	3	1	50	
	rech_del6	days	3	1	50	
	rech_del7	days	3	1	50	
	kaquifer01	m/day	8.64E-05	8.64E-07	0.00864	
	kaquifer02	m/day	0.005	5.00E-05	0.49999999	
	kaquifer03	m/day	0.00864	8.64E-05	0.86399997	
	kaquifer04	m/day	0.0864	8.64E-04	8.64	
	kaquifer05	m/day	**1**	**0.01**	**10**	
	kaquifer06	m/day	5	0.05	15	**1.75**
	kaquifer07	m/day	15	0.15	15	
	syaquif_01		**0.05**	**5.00E-04**	**0.5**	
	syaquif_02		0.05	5.00E-04	0.5	**0.077**
	syaquif_03		0.05	5.00E-04	0.5	
	syaquif_04		0.05	5.00E-04	0.5	
	syaquif_05		**0.25**	**2.50E-03**	**0.5**	
	syaquif_06		0.3	3.00E-03	0.5	**0.4**
	syaquif_07		**0.15**	**1.50E-03**	**0.5**	
	bed_k1	m/day	8.64E-08	8.64E-09	8.64E-07	**5.78E-02**
	bed_k2	m/day	5.00E-06	5.00E-07	5.00E-05	
	bed_k3	m/day	8.64E-06	8.64E-07	8.64E-05	
	bed_k4	m/day	8.64E-05	8.64E-06	8.64E-04	
	bed_k5[1]	m/day	**0.001**	**1.00E-04**	**0.01**	**1.75E-03**
	bed_k6	m/day	0.005	5.00E-04	0.05	
	bed_k7	m/day	**0.015**	**0.0015**	**0.15**	**0.051**
	bed_depth	**m**	**5**	**0.5**	**10**	**7.32**
	bed_thick	**m**	**0.5**	**0.2**	**2**	**0.22**
gwflow.tile	tile_depth	m	1.22	4	0.5	
	tile_area	m^2	50	2500	10	
	tile_k	m/day	5	20	1	
gwflow.floodplain	kfloodpln1	m/day	15	17	4	
	kfloodpln2	m/day	1	7	0.01	
	kfloodpln3	m/day	0.005	0.08	5.00E-04	
	kfloodpln4	m/day	8.64E-05	4.90E-04	1.00E-06	
gwflow.canal	canal_k_01	m/day	5.00E-04	5	1.00E-05	
	canal_k_02	m/day	5.00E-04	5	1.00E-05	
	canal_k_03	m/day	5.00E-04	5	1.00E-05	

	canal_k_04	m/day	5.00E-04	5	1.00E-05	
	canal_k_05	m/day	5.00E-04	5	1.00E-05	
	canal_k_06	m/day	5.00E-04	5	1.00E-05	
	canal_k_07	m/day	5.00E-04	5	1.00E-05	
	canal_k_08	m/day	5.00E-04	5	1.00E-05	
	canal_k_09	m/day	5.00E-04	5	1.00E-05	
	canal_k_10	m/day	5.00E-04	5	1.00E-05	
	canal_k_11	m/day	5.00E-04	5	1.00E-05	
	canal_k_12	m/day	5.00E-04	5	1.00E-05	
	canal_k_13	m/day	5.00E-04	5	1.00E-05	
	canal_k_14	m/day	5.00E-04	5	1.00E-05	
	canal_k_15	m/day	5.00E-04	5	1.00E-05	
parameters.bsn	**scoef1**		**1**	**0.05**	**24**	**0.8**
hyd-sed-lte.cha	k_mainstem	mm/hr	1	10	0.001	
	manningmst[2]		**0.05**	**0.005**	**0.3**	**0.074**
snow.sno	temp_lag__	days	1	0.01	1.01	
	melt_max__	°C	4.5	1.4	6.9	
	melt_temp_	°C	0.5	0	5	
topography.hyd	slp_len10	m	10	10	150	
	slp_len30	m	30	10	150	
	slp_len60	m	60	10	150	
	slp_len90	m	90	10	150	
	slplen121	m	121	10	150	
soils.sol	awc11		0.04	0.01	1	
	awc12		0.03	0.01	1	
	awc21		0.16	0.01	1	
	awc22		0.19	0.01	1	
	awc31		0.06	0.01	1	
	awc32		0.01	0.01	1	
	awc41		0.13	0.01	1	
	awc51		0.03	0.01	1	

*Zone 5 streambed hydraulic conductivity was further manually iterated to .00067 m/day

**Mainstem manning's n was further iterated to 0.01 for channel reaches 1-6, and 0.02 for all other reaches.

2.4 Flood Scenarios

Flood scenarios were created to excite floodplain processes and compare floodplain recharge magnitudes to other groundwater fluxes within the region. The Log Pearson (III) method from Bedient et al. 2002 was used to calculate discharges for a 100-year and 500-year

return periods (Table 3) from annual maximum streamflow of all available USGS data for each tributary used as a SWAT+ point source inlet.

Table 3: 100-year and 500-year discharge volumes for tributaries used in scenarios.

		Inlet Log Pearson II Maximum Discharge						
		Pueblo	**Fountain**	**St Charles**	**Huerfano**	**Timpas**	**Apishpa**	**Horse**
500 Year	CMD	83,200,000	59,200,000	12,700,000	12,100,000	12,400,000	8,140,000	11,700,000
	CFS	34,015	24,200	5,170	4,950	5,060	3,330	4,780
100 Year	CMD	57,100,000	32,100,000	8,630,000	8,210,000	7,430,000	5,760,000	4,590,000
	CFS	23,300	13,100	3,530	3,360	3,040	2,360	1,880

Flood event peak discharges were fit to the existing series of daily inlet streamflows by ramping up to the peak discharge seven days then ramping back to zero over the next twenty-three days. Flood distributions were then intersected over the existing inlet hydrographs (Figure 7). Point source files were created for both 100-year and 500-year events to simulate the hypothetical floods, set to occur in October of 2012 and May 2015.

For future reference, scenarios will be referenced as:

Basecase – Calibrated model with original point source data. Floodplain flag turned on.

SP500, fplnSP500 – The calibrated model run with a 500-year flood event from each tributary occurring in May, 2015. Floodplain flag turned **on**.

nflgSP500 – The calibrated model run with a 500-year flood event from each tributary occurring in May, 2015. Floodplain flag turned **off**.

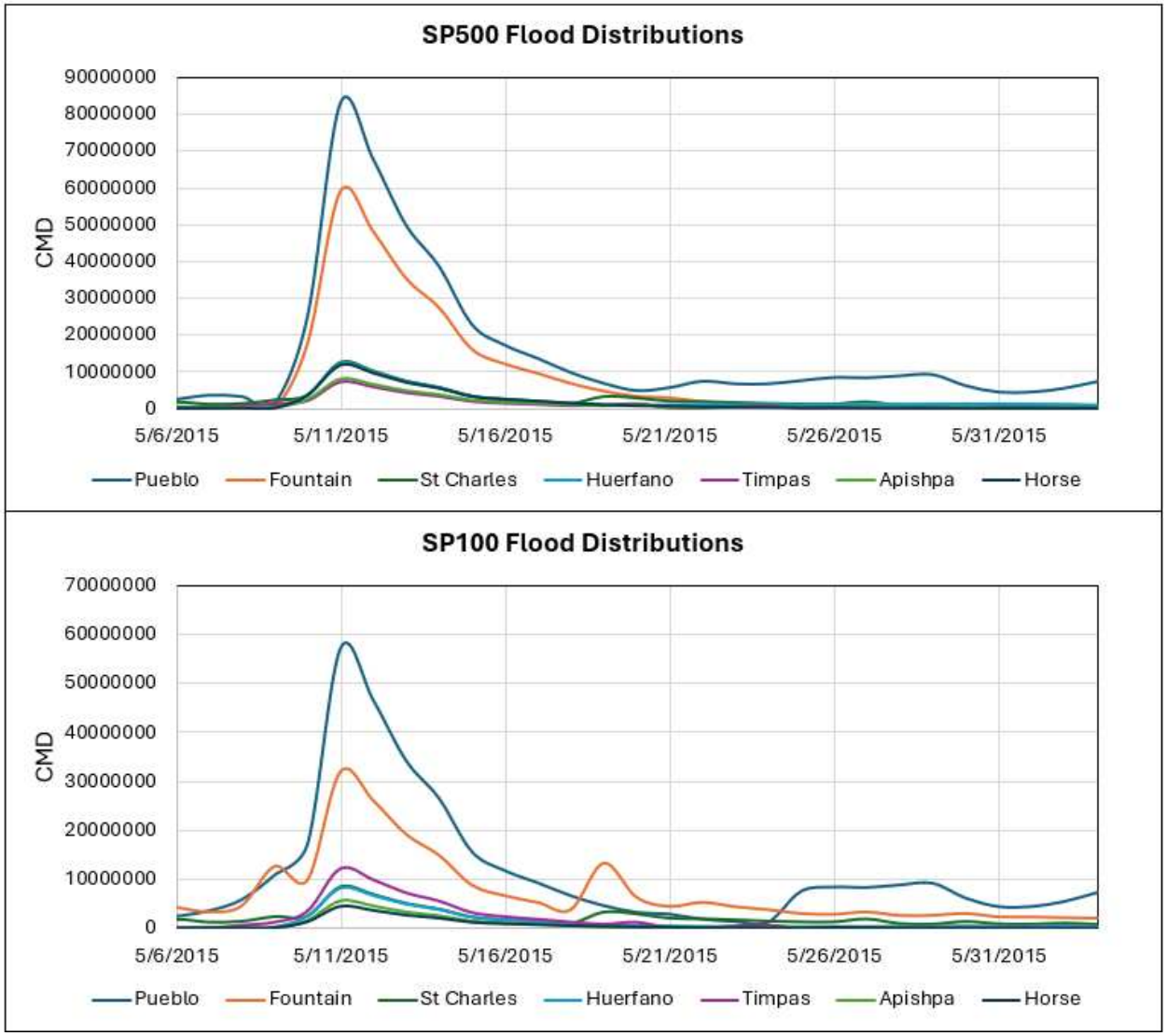

Figure 7: Modeled inlet streamflow distributions for the 100-year and 500-year flood scenarios.

3. RESULTS AND DISCUSSION

3.1 Model Performance

Sensitivity analysis and calibration highlighted parameters related to streamflow at the outlet, controlling processes such as surface runoff and groundwater-stream exchange. Curve numbers and coefficients controlling surface runoff and aquifer properties for alluvium in geologic zone #5 (Table 2) were identified as most significant. Other parameters that may be consequential to specific water balance components but not streamflow were not calibrated. Parameters fell within expected ranges of what is realistic to the region and the physical process (Abbas et al. 2024).

Calibration was performed with the default irrigation depth of 25.4 mm/day (1 inch/day) for both practices which is at the lower end but within the range of irrigation estimates for the LARV (Gates et al. 2006; Gates et al. 2012). Higher irrigation depths (80 mm/day) were tested but resulted in very high streamflow estimates.

3.1.1 Streamflow

Streamflow values from the end of the full 1992-2020 simulation period were plotted alongside observed flows from the outlet in Las Animas and five additional validation gauges. A Nash-Sutcliffe Efficiency (NSE) was calculated to quantify model performance at monthly time steps (McCuen et al. 2006) for the calibration period from 1992-2007, and a testing period from 2008 through the end of the simulation (Figure 8, 9).

Upstream validation stations at Avondale and Nepesta calculated higher NSE values, explained by proximity to measured streamflow inputs at inlet point source stations. Model performance continues to weaken toward the outlet at Las Animas (calibration NSE = 0.32,

testing NSE 0.00), but simulated streamflows are still acceptably close to observed values as far downstream as Rocky Ford (calibration NSE = 0.65, testing NSE 0.39) for analysis. NSE values are overall higher during the calibration than the testing period. It is difficult to identify whether an error was made during calibration or while creating the water allocation and diversion files, considering the LARV is a highly managed watershed with many users (Triana et al. 2010). In addition, the SWAT+ initialization in QSWAT discretized the channel into long reaches with endpoints that are not necessarily close to validation gauges.

Original calibration overestimated streamflow at downstream stations with an observable lag between seasonal streamflow peaks. Manual parameter iterations were completed, settling on lower zone 5 streambed hydraulic conductivity and manning's n values.

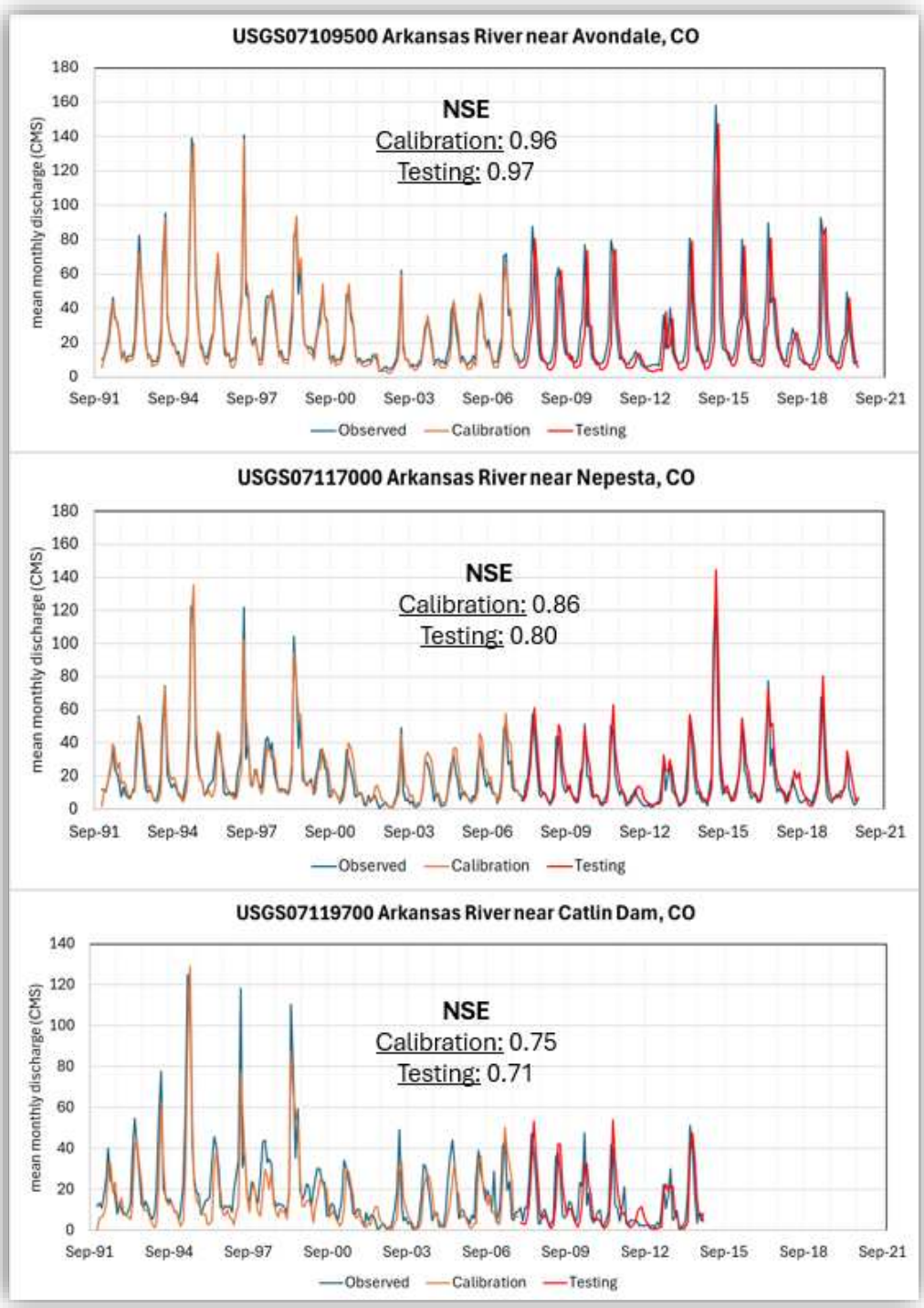

Figure 8: Comparison of simulated and observed streamflows at gaging station locations: Avondale (top), Nepesta (middle), Catlin Dam (bottom). Streamflows are plotted for the 1992-2007 calibration period and the testing period from 2008 to 2020, along with corresponding Nash-Sutcliffe Efficiency values. See Figure 2 for validation gauge locations.

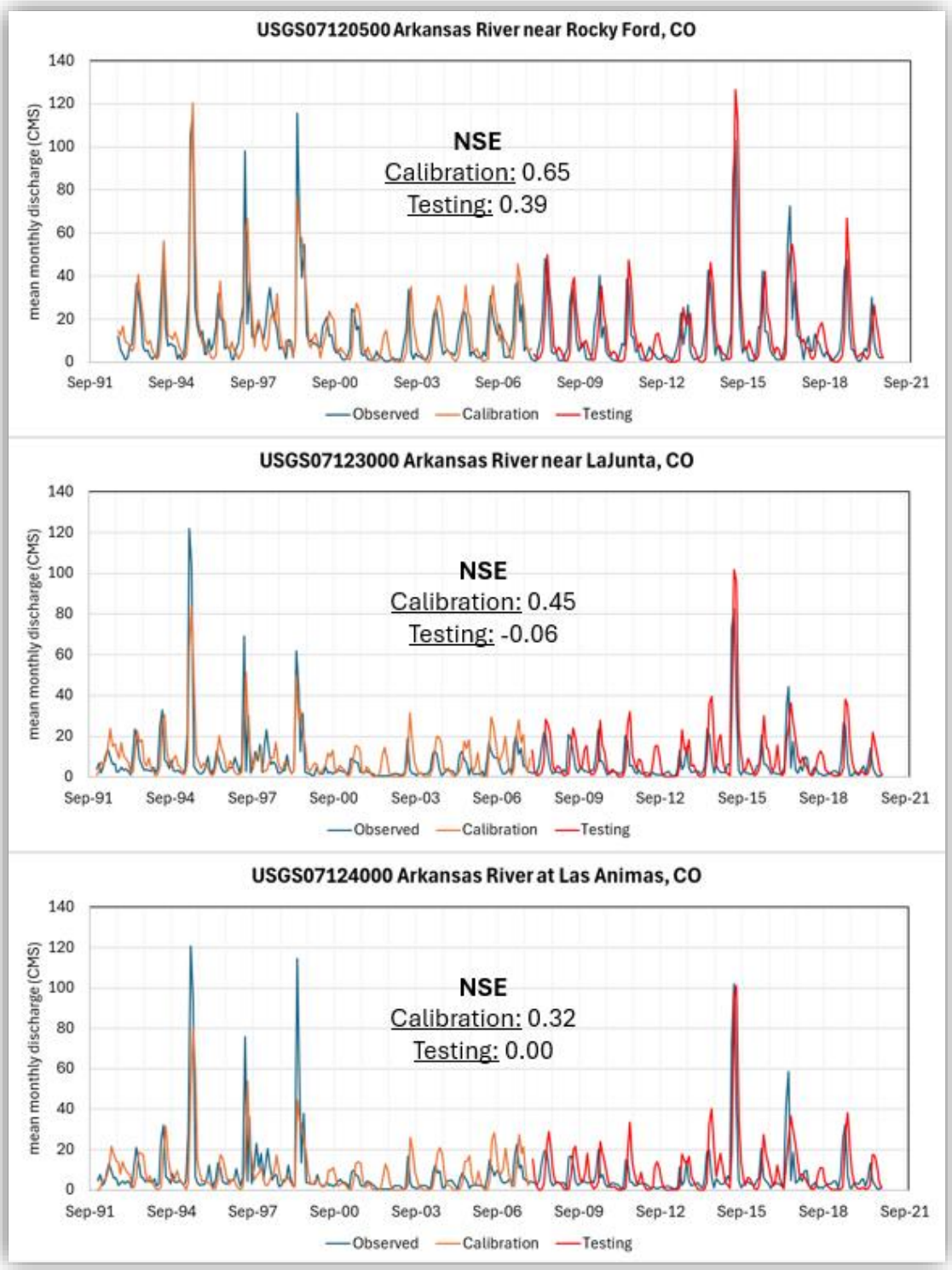

Figure 9: Comparison of simulated and observed streamflows at gaging station locations: Rocky Ford (top), La Junta (middle), Las Animas (bottom). Streamflows are plotted for the 1992-2007 calibration period and the testing period from 2008 to 2020, along with corresponding Nash-Sutcliffe Efficiency values. See Figure 2 for validation gauge locations.

3.1.2 Groundwater

Modeled groundwater heads were compared with USGS observations from thirteen wells in unconsolidated alluvium and Quaternary gravels (geologic zones 5 and 7, Figure 4). Groundwater observation data were given in measurements of depth-to-water from the ground surface, which were subtracted from the *gwflow* ground surface to align datums for analysis. Modeled heads are under-projected in alluvium (3.4-5.6 m mean error) and over-projected in Quaternary gravels (0.7-7.4 m mean error). Observed heads had a range of 217 m and mean absolute error (MAE) of modeled heads calculated to 3.46 m for a MAE/Range = 1.6 %. The MAE/Range is relatively low, but a goal of calibration was to model groundwater heads within 0-2 m of observed values. Figure 10 shows modeled hydraulic heads plotted against measurements from observation wells.

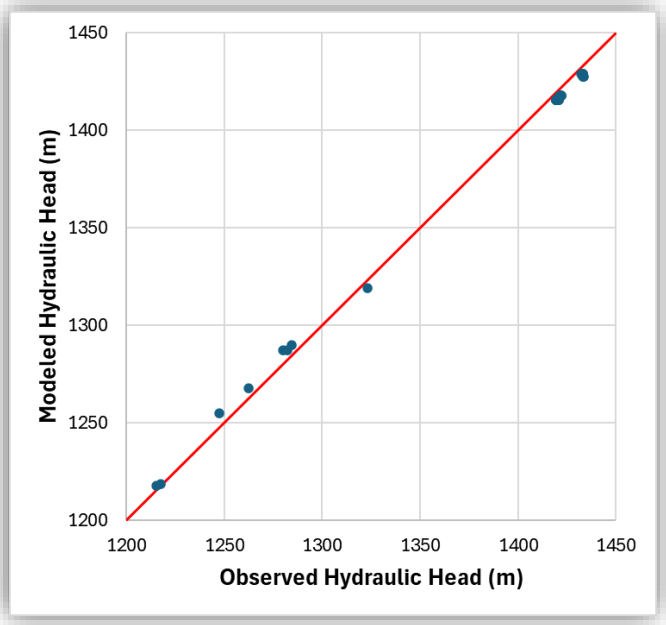

Figure 10: Modeled hydraulic heads plotted against corresponding observed heads with a 1:1 line. Observation wells drilled in alluvium with underestimated hydraulic heads are higher in the watershed than the overestimated heads with targets in Quaternary gravels. Observation well locations are marked in Figure 4.

Initial conditions are important for accurate groundwater head calculations (Zhou and Li 2011). In the absence of a steady-state model to import initial conditions, the full transient simulation was run before analyzing model output with the groundwater head initial condition of 5 m below the surface (Ajami et al. 2015). Various initial depths to groundwater were tested to address error in different regions of the model domain, but groundwater levels continued to equalize at or near the original deviation from observations. Different hydraulic conductivity values were tested, irrigation depths were increased to 80 mm (Gates et al. 2012), and canal hydraulic conductivity was increased (Almahawis et al. 2024), but groundwater head accuracy did not improve.

Modeled hydraulic head distribution across the valley follows an expected trend downward through the watershed, as shown in Figure 11. The *gwflow* module only enables a no-flow or constant head boundary condition for all boundary cells, multiple boundary conditions cannot be set. There was concern that the no-flow boundary condition would affect modeled heads in the alluvial aquifer adjacent to inlet point sources where the watershed area had been clipped. This concern was dismissed since there is no observable effect, and the study is focused on the corridor along the Arkansas River mainstem.

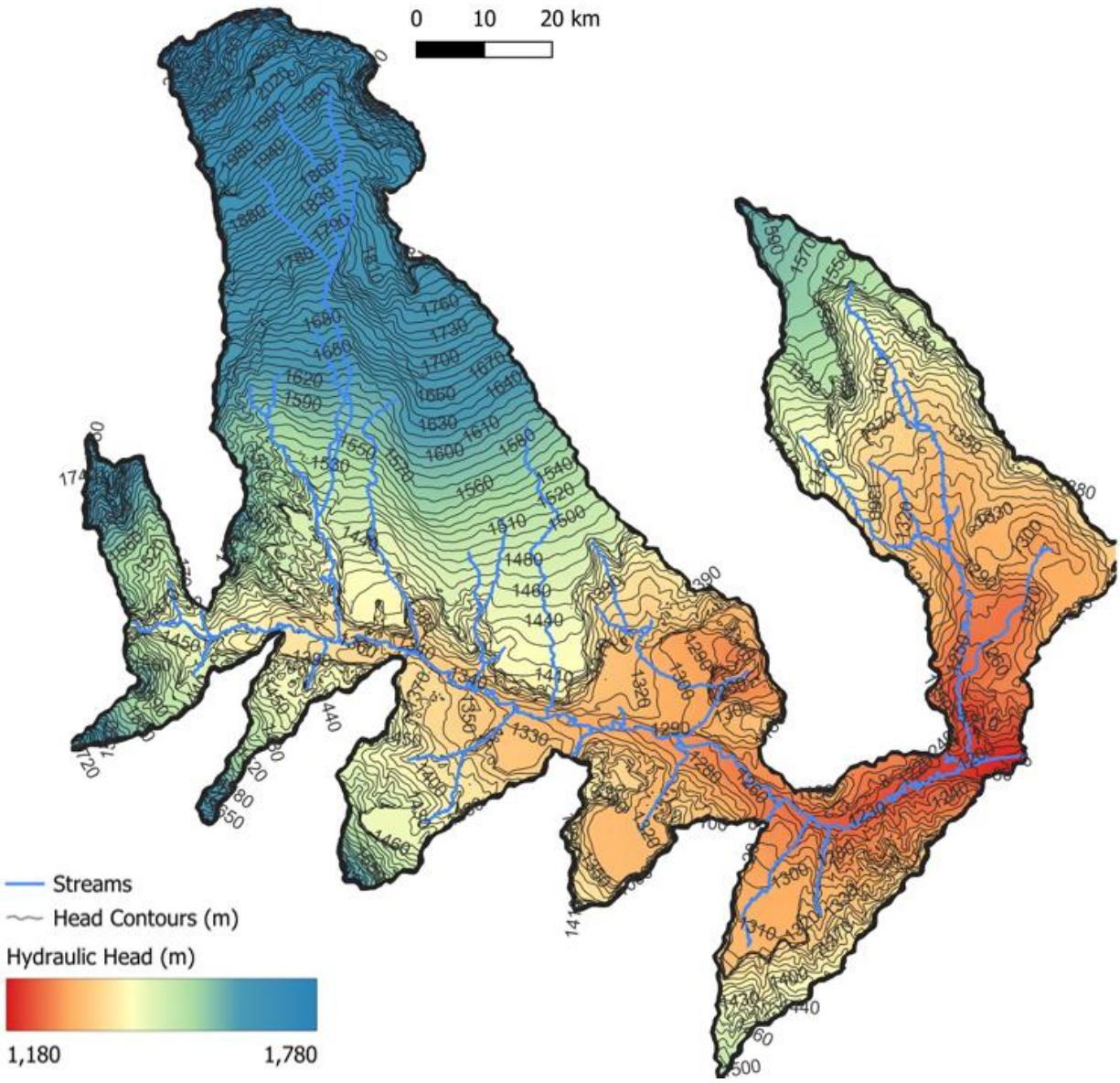

Figure 11: 2015 simulated hydraulic heads plotted for the basin.

3.2 Water Balance

3.2.1 Groundwater Balance

The annual groundwater balance in Figure 12 displays active fluxes from 1999 through 2020 and annual changes in groundwater volume. Groundwater pumping and upflux to the soil profile account for the greatest losses of groundwater, while stream seepage provides the most recharge. Recharge from deep percolation through the soil profile is considerable at 43 to 94

mm/year active and is largely influenced by irrigation (Buffaut et al. 2020) but is masked by exchanges to the HRU soil profile component of net recharge. Note that water upflux to the HRU soil profile may be further removed from the basin as evapotranspiration in SWAT+ routines, groundwater evapotranspiration is a separate process that removes water directly from the saturated zone when hydraulic heads exceed the gwet 2 m extinction depth from ground surface. Other studies estimate the total upflux from the aquifer to soil and evapotranspiration to be within 5 mm/day in summer months in irrigated areas of the LARV (Morway et al. 2006). All components listed in the Figure 12 legend are nonzero. Canal seepage is minuscule due to the small canal bed hydraulic conductivity of 0.0005 m/day and its total flux is vastly underestimated in comparison with other studies that estimate canal hydraulic conductivity in the LARV between 0.4 and 0.026 m/day (Gates et al. 2006; Susfalk et al. 2008). Increasing canal hydraulic conductivity greatly overestimated modeled streamflow at the model outlet so no changes were made. The accurate simulation of canal seepage should be addressed in future work. However, this likely does not have a strong impact on floodplain-channel processes.

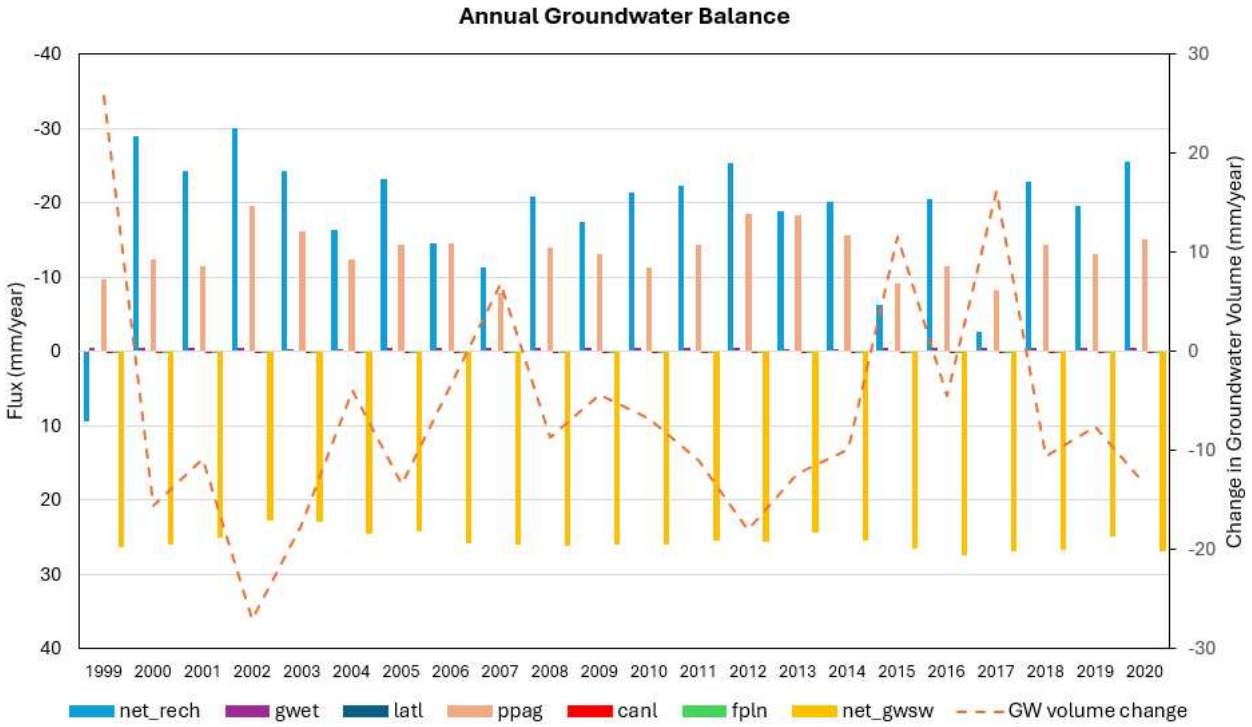

Figure 12: Annual groundwater balances from 1998 through 2020. Refer to the key in Table 1 for descriptions of active fluxes. Net_rech = recharge - soil transfer; net_gwsw = sw → gw – gw→sw.

Most years of the simulation report a net loss in groundwater volume. The basin-wide net and directional fluxes in net groundwater-stream exchange remain relatively constant. Still, a decrease in total flux from streams toward the aquifer is observed following the drought simulated in 2012 (185 mm/year). Years with losses in groundwater storage are most likely a product of increased losses to pumping, reduced net recharge, and reduced discharge from the stream to aquifer. Highest observed streamflows during the simulation period occur in 1999, 2015, and 2017, which coincide with the greatest increases in groundwater storage. Again, with small changes in net groundwater-stream exchange, additional recharge and pumping reductions are responsible for increased groundwater storage. Average total recharge, pumping, basin evapotranspiration, and surface runoff are within expected ranges for this region estimated by

empirical regressions by Reitz et al (2013), but soil moisture upflux from the aquifer is a larger portion of the water balance in this model.

A flux hydrograph was created using the methods described in Bailey et al. 2022 to inventory processes that contribute to streamflow (Figure 13). Surface runoff is responsible for the large majority of basin discharges to channels with very little lateral flow discharging from the soil profile. Groundwater discharges are considerable streamflow contributions, simulated at 135 m^3/s for August of 2017, and seasonally increase by a factor of 3 to 4 with no observable lag behind seasonal surges in surface runoff. The timing of recharge processes likely coincides with overall increases in surface runoff, suggesting a highly conductive alluvial aquifer.

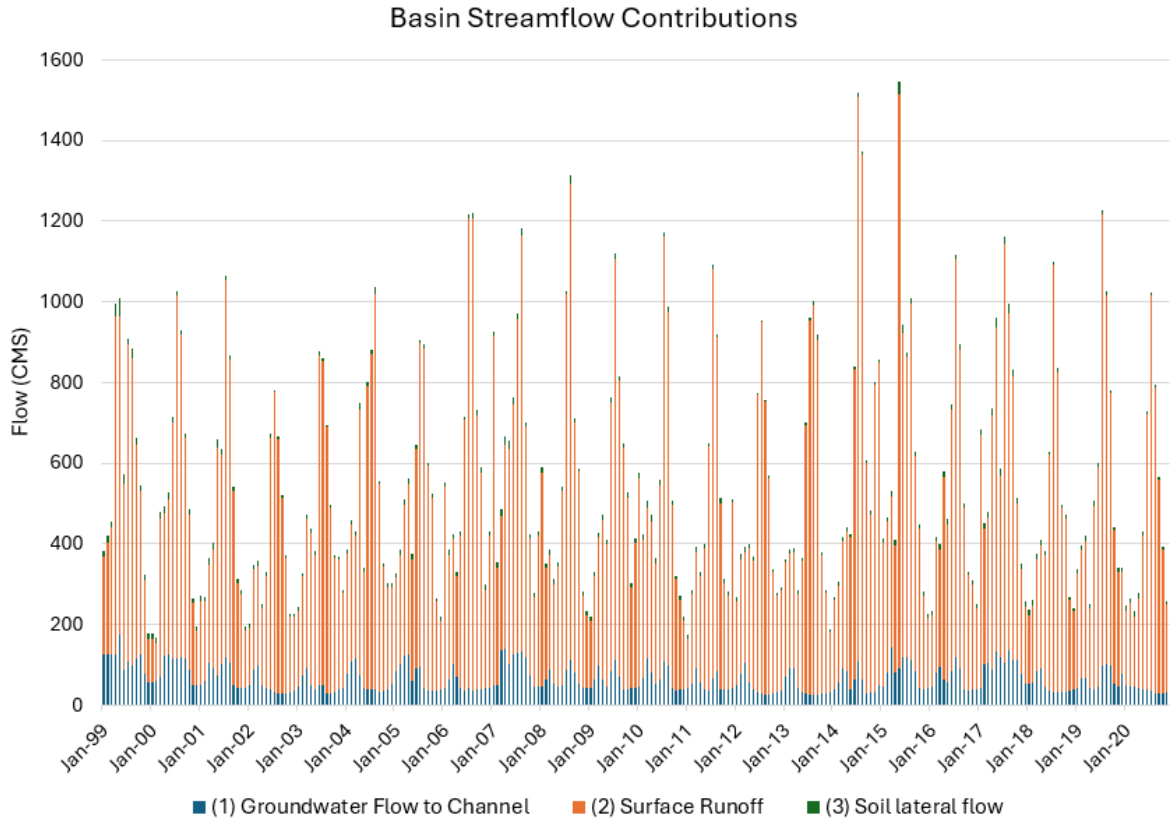

Figure 13: The hydrographs below sum the monthly discharges from the basin's hydrologic processes contributing to streamflow. Total flows to channels include (1) groundwater contributions, (2) surface runoff, and (3) unsaturated zone discharges. Groundwater contributions include groundwater to surface water exchange, saturation excess flow, and tile drainage. No processes that remove surface flows are included.

3.2.2 Groundwater Fluxes

Maps of cell-by-cell annual average discharges for several groundwater processes in the simulation year 2015 are included in Figures 14-16. As mentioned in section 3.2.1, canal seepage is largely underestimated, but the majority of canal cells are leaking with several isolated cells receiving groundwater where the water table elevation exceeds canal elevations.

The USFW shapefile for riparian ecosystems mapped several landscapes on low-order streams. Although no simulated overbank flow conditions activated floodplain-aquifer exchange along the mainstem Arkansas River corridor, floodplain processes are active higher in the watershed.

Groundwater evapotranspiration is primarily active through the irrigated alluvial valley where the shallow water table is presumably near or above the 2 m groundwater extinction depth (Niemann et al. 2011). The gwet routine does not capture evapotranspiration from cottonwood trees and other phreatophytes continuously rooted below the water table (Busch et al.1992).

Minor recharge inflows are mapped in upland areas, but highest recharge rates are mapped along the irrigated corridor, particularly near the confluence of Horse Creek. Please note that the recharge map in Figure 15 does not include losses to the soil profile as calculated in the groundwater balance.

Channel cells show continuous exchange with the aquifer along the Arkansas River. Most cells report surface water entering the aquifer with isolated downstream cells discharging to the river. Most low-order streams show discharge to channels or low flows to groundwater. Inactive channel cells are expected to represent ephemeral streams.

Groundwater pumping is widespread through the irrigated valley. Pumping is active within the reach of all irrigation supply canals, but withdrawals are least (<600 m3/day) in these

areas. Most groundwater pumping occurs in the reach between the St. Charles and Huerfano Rivers, where few minor irrigation ditches cross the landscape.

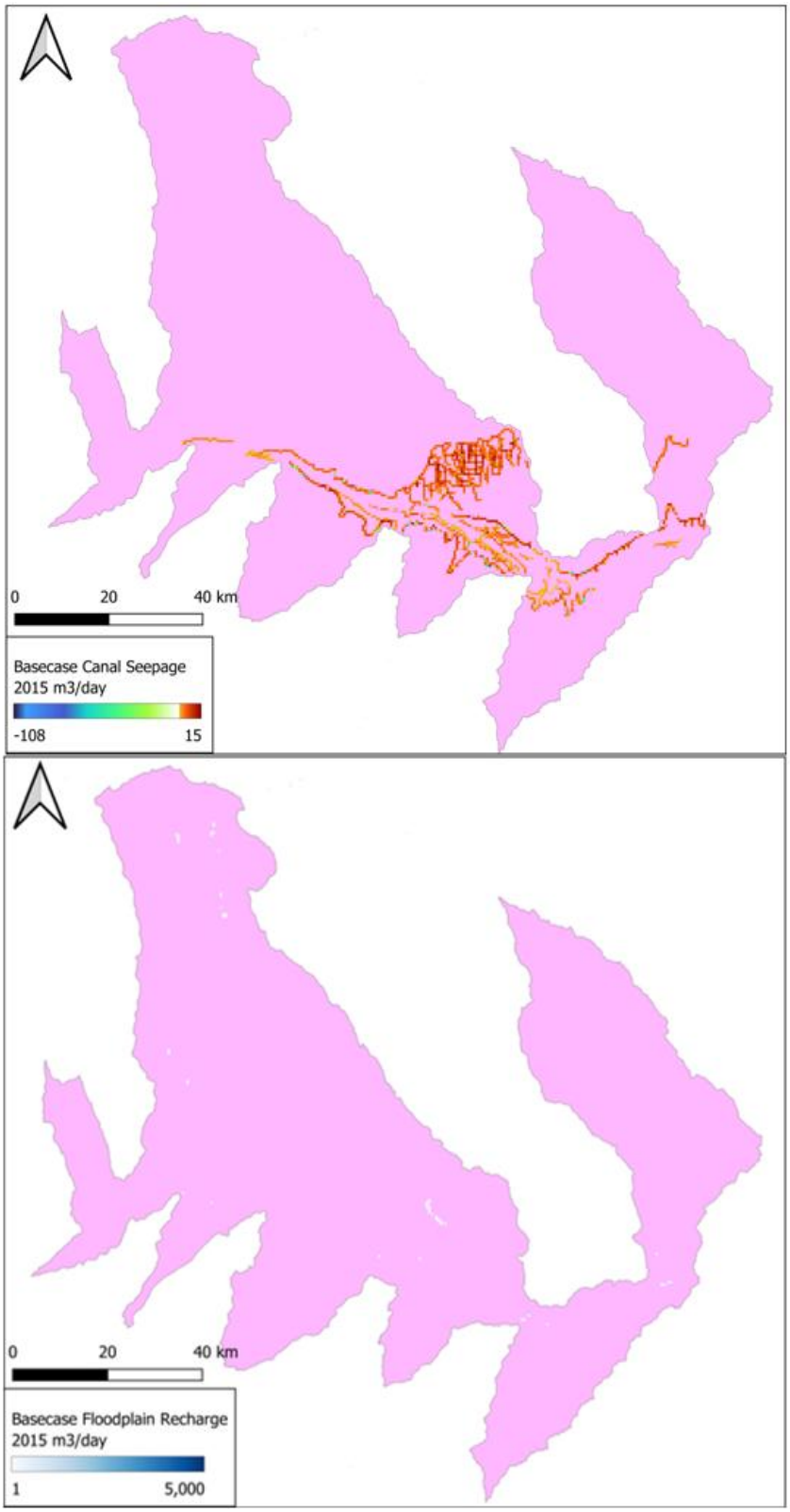

Figure 14: Maps show discharges from canal seepage (top) and floodplain exchange (bottom) in simulation year 2015 of the *Basecase* scenario.

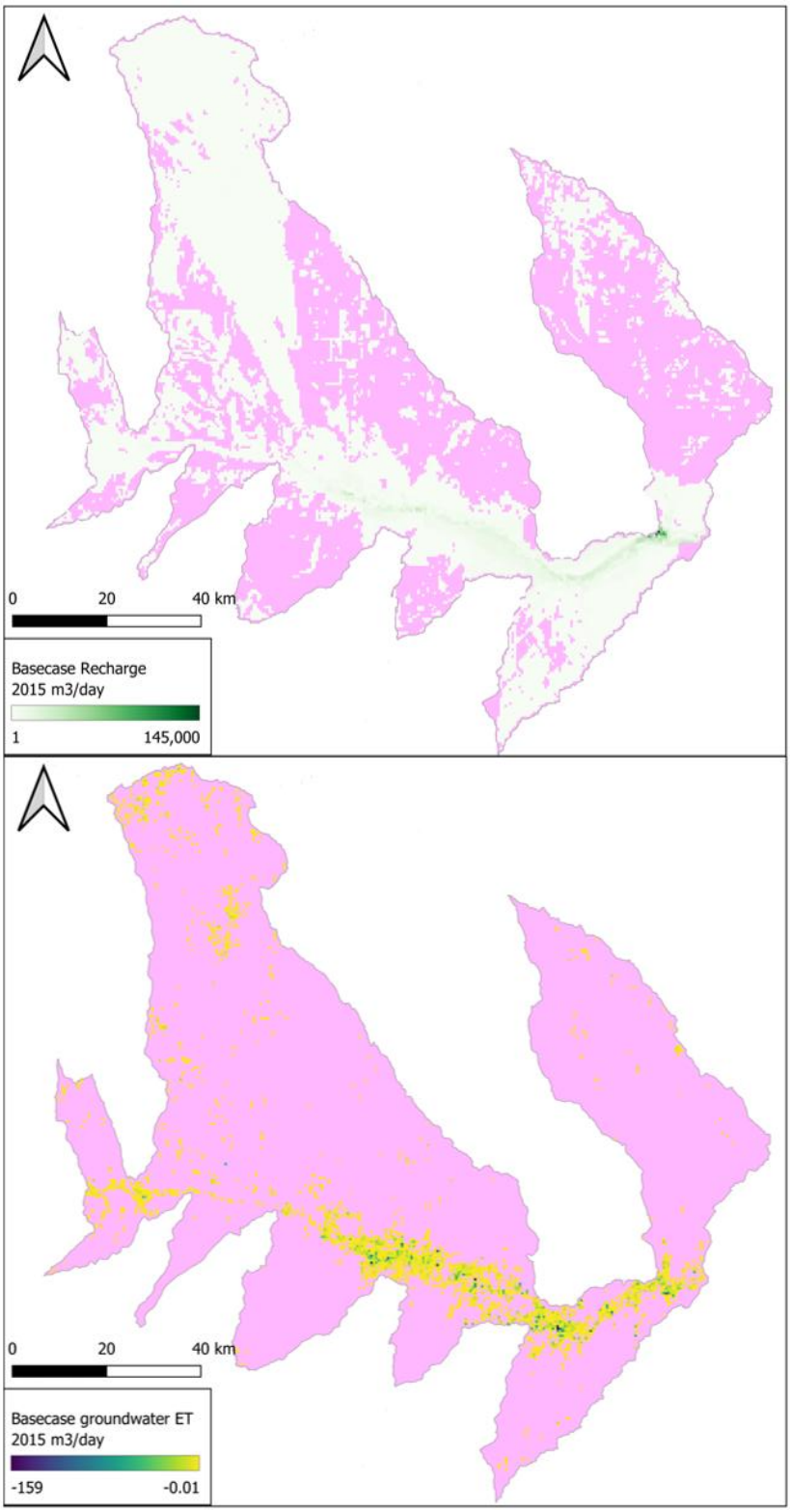

Figure 15: Maps show discharges from deep percolation (recharge, top) and groundwater evapotranspiration (bottom) in simulation year 2015 of the *Basecase* scenario.

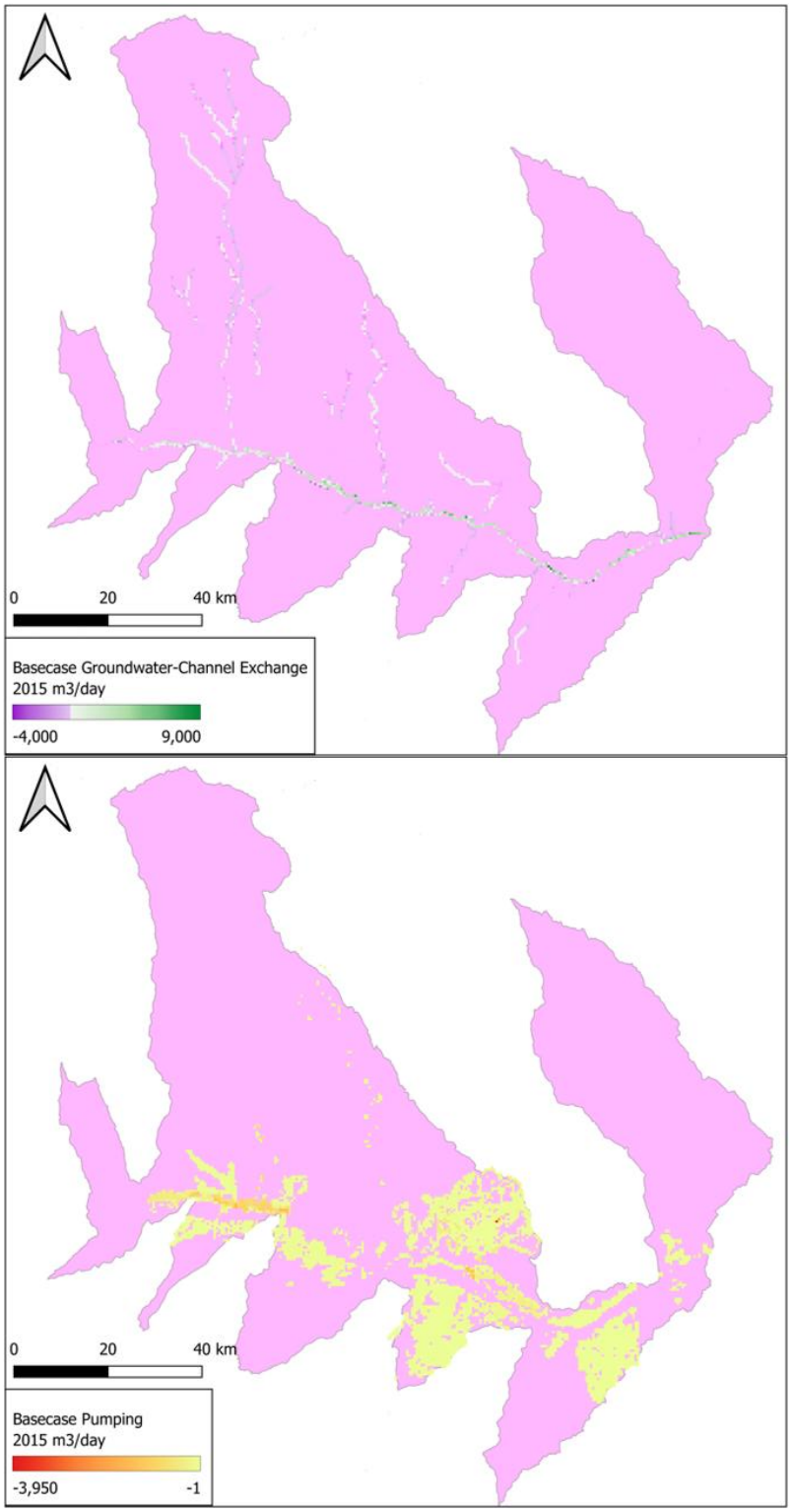

Figure 16: Maps show discharges from groundwater-stream exchange (top) and pumping (bottom) in simulation year 2015 of the *Basecase* scenario.

3.3 Flood Scenario Results

The 100-year and 500-year flood distributions described in Section 2.4 were each tested in October 2012 and May 2015. All scenarios activated groundwater-floodplain exchange, with the 500-year event occurring in May of 2015 (SP500) activating the most cells and reporting the highest floodplain flux. Since the 500-year event is a discharge instead of a storm, the May scenario was also selected for wetter conditions and higher soil moisture.

3.3.1 Floodplain Exchange

The maps in Figure 17 show cells available to *gwflow* floodplain processes with the 2015 SP500 floodplain exchange rates. Overbank flow stimulated floodplain recharge just beyond Catlin Dam, but did not activate further toward Rocky Ford. SWAT+ river routing routines calculate overbank flow from bank depth, width, and daily discharge per channel reach with processes accounting for flood storage volume conveyance (Tull and Passalacqua 2025; Wohl 2021). Floodplain delineation is not continuous through the entire Arkansas River corridor. It is possible and likely that surfaces flood but are not delineated for floodplain exchange with the aquifer. Active floodplain cells follow the river corridor in a narrow path, largely just one to two cells wide across the valley; north-to-south spans of two or more active cells are typically surrounding river beads (Schultz et al. 2024; Wohl 2021). The narrow band of activated floodplain cells suggests that overbank flows do not extend far across the valley. Artificial levees, such as those observed in satellite imagery along the Arkansas River through the town of Pueblo, CO, constrain flood flows to channels (Knox et al. 2018). Levees were not considered in floodplain cell delineation, but do not appear to be present downstream of Pueblo, CO.

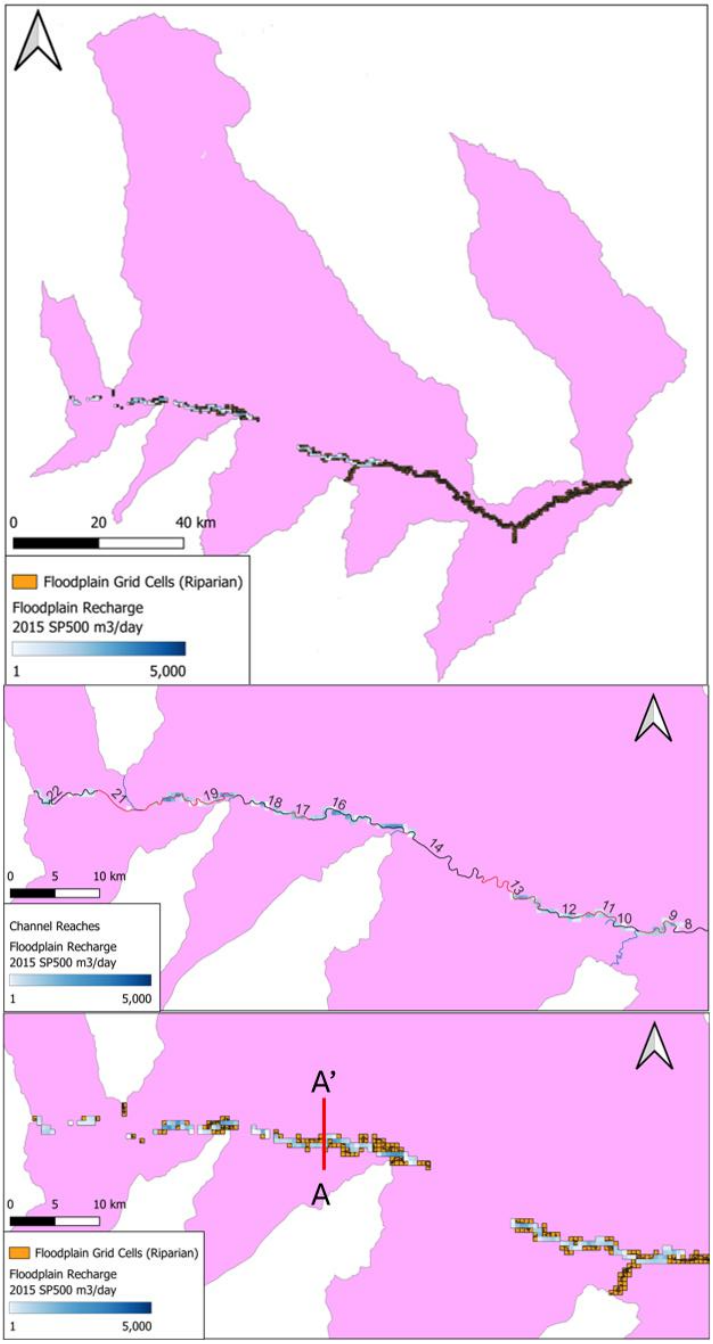

Figure 17: Maps show floodplain exchange during the 2015 scenario for (top) the entire watershed, (middle) with channel reaches labeled, (bottom) displaying inactive floodplain cells.

3.3.2 Effect of *gwflow* Floodplains

Additional testing ran the SP500 scenario with *gwflow.input* floodplains turned on (fplnSP500) and off (nflgSP500). Implications to the groundwater and surface water balances for

the entire basin are summarized in Table 4 and Table 5 respectively. Integrating floodplains into the model for a flood scenario added 4.47 mm of recharge from floodplain exchange, overall increasing groundwater storage by 2 mm. Additional processes affecting groundwater storage include decreases in stream seepage and net recharge, additional losses to saturation excess flow, and reduced groundwater pumping. The SWAT+ basin water balance is affected by 1-2 mm/year decreases in surface runoff and irrigation, and an additional 34 mm of deep percolation.

Table 4: Scenario comparison of basin-wide groundwater balance components.

		Basecase	**fplnSP500**	**nflgSP500**	*effect of flood*	*effect of fpln flag*
	Year	**Average**	**2015**	**2015**	*scenario*	
mm/yr	**dVol**	-6.0	13	11	Increase	Increase
mm/yr	**net_rech**	-18	-8.0	-6.3	Decrease	Decrease
mm/yr	**gwet**	-0.49	-0.50	-0.49	Increase	Increase
mm/yr	**sw-gw**	26	27	28	Decrease	Decrease
mm/yr	**satx**	-0.35	-1.5	-0.92	Increase	Increase
mm/yr	**latl**	0	0	0	None	None
mm/yr	**ppag**	-13	-9.1	-9.3	None	Decrease
mm/yr	**tile**	-0.18	-0.26	-0.25	Increase	Increase
mm/yr	**canl**	0.16	0.16	0.16	None	None
mm/yr	**fpln**	0.02	4.47	0	Increase	Increase

Table 5: Scenario comparison of SWAT+ basin water balance components

		Basecase	**fplnSP500**	**nflgSP500**	***effect of flood***	***effect of fpln flag***
	Year	**Average**	**2015**	**2015**	***scenario***	
mm/yr	precip	335	430	430	None	None
mm/yr	surq_gen	49	55	56	Decrease	Decrease
mm/yr	latq	1.0	1.3	1.2	Increase	Increase
mm/yr	perc	675	842	808	Increase	Increase
mm/yr	et	347	418	417	Increase	Increase
mm/yr	sw_ave	50	54	53	None	Increase
mm/yr	sw_chang	-3	2	2	None	None
mm/yr	irr	47	37	39	Decrease	Decrease

Table 6: Summary of floodplain processes on the flux hydrograph.

		May		October		Immediate fpln effect	6 Month fpln effect
		fplnSP500	nflgSP500	fplnSP500	nflgSP500		
Surface Runoff	**m3/s**	**1384**	**1418**	**413**	**418**	Decrease	Increase
Soil Lateral Flow	**m3/s**	**34.0**	**31.3**	**9.49**	**8.90**	Increase	Increase
Net GW Contributions	**m3/s**	**121**	**46.1**	**35.4**	**34.1**	Increase	Increase
GW → Streams	m3/s	46.0	32.7	31.8	30.2	Increase	Increase
Saturation Excess	m3/s	71.4	10.6	1.9	1.9	Increase	
Tile Drainage	m3/s	3.25	2.80	1.8	2.0	Increase	Decrease
Net Flux Hydrograph	m3/s	1538	1496	458	461	Increase	Decrease

Including floodplain processes greatly increased groundwater discharge to channels by nearly a factor of three, providing evidence that floodplains may play a major role in groundwater-surface water interactions (Saksena et al. 2017). Saturation excess flow increased by a factor of 7, while discharge through streambeds and tile drainages also increased considerably. Despite minor reductions in surface runoff and unsaturated zone flow, the net flux hydrograph totals (Table 6) higher flows when integrating floodplains to groundwater models with bankfull events. An interesting finding is that six months after flooding, monthly average streamflow contributions are estimated lower than standard models without floodplain processes.

Integrating floodplains into SWAT+ *gwflow* models has a strong impact on local hydraulic head distributions. The maps in Figure 18 show the difference between hydraulic heads output from the SP500 scenario with and without the *gwflow.input* floodplain flag for May and October 2015. Modeled hydraulic heads are 6 m higher in areas following the flood event, and

remain elevated beyond six months with active floodplain exchange. Floodplain exchange in low-order streams also outputs higher heads, but residuals dissipate toward standard transient conditions sooner. A lower water table (<1 m) was identified in a small cluster of cells south of Nepesta and remains unexplained.

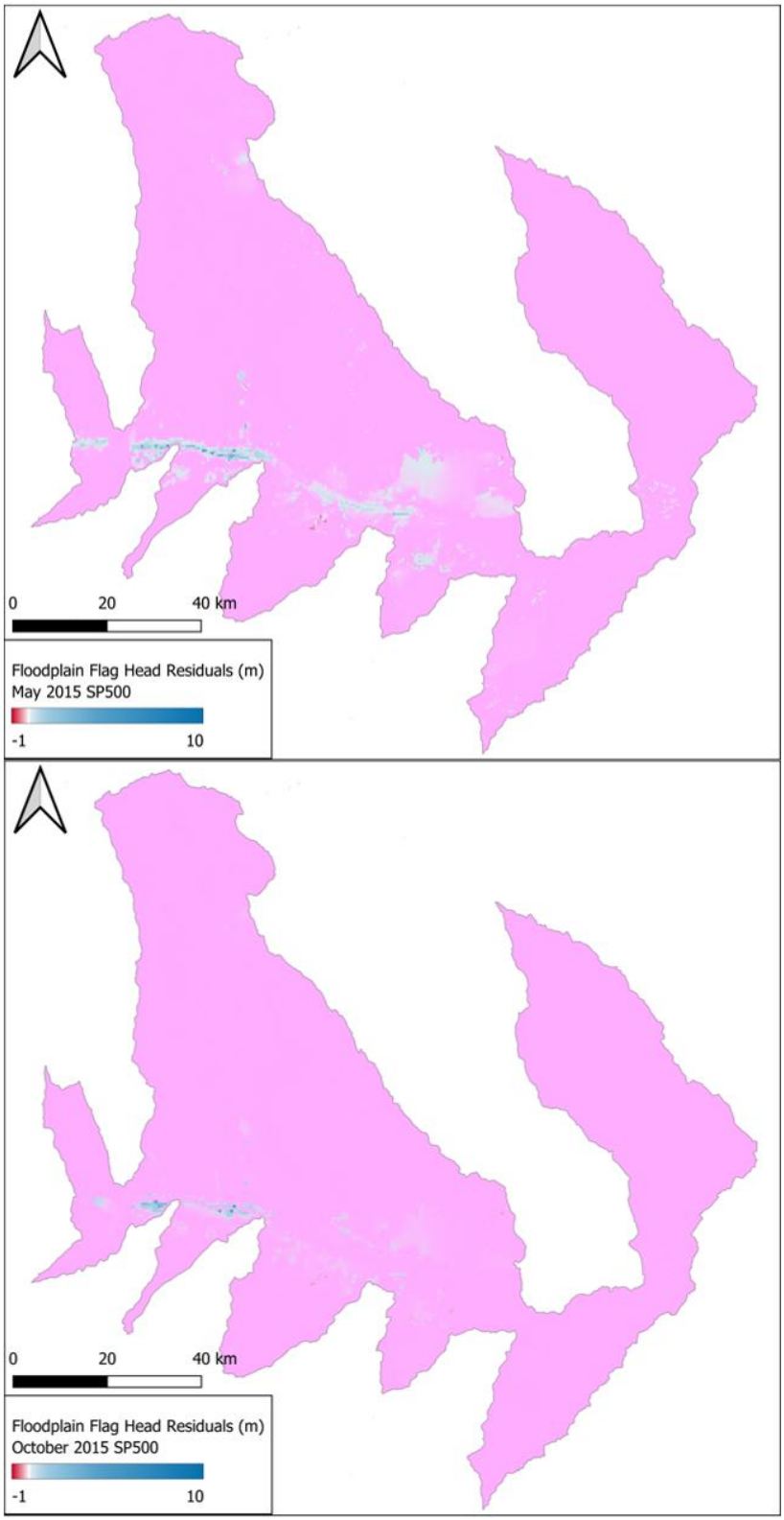

Figure 18: Maps show hydraulic head residuals calculated as the head difference from model outputs using and without using the floodplain flag for May (top) and October (bottom) 2015 of the SP500 scenario.

Similar maps of fplnSP500-nflgSP500 residuals in Figure 19 show the effect of integrating floodplains on other groundwater exchange processes. Increased groundwater evapotranspiration occurs proximal to the downstream string of active floodplains. Recharge flows increase by large amounts at and surrounding floodplain cells extending up-valley in smaller amounts. Saturation excess flows activate at and near active floodplains, a *gwflow* process that remained entirely dormant without floodplain exchange.

Floodplains are known to store groundwater flows from higher in the basin (Cartwright et al. 2019) and discharge to streams depends on fluctuating stream stage (Jolly and Rassam 2009). Darcy's law formatted for floodplain exchange intends to discharge from the aquifer to floodplains when the water table exceeds the ground surface (Schultz et al. 2024), but a discharge of groundwater to floodplains was not recorded in any instances. It is likely that *gwflow* code transfers activate saturation excess flow and groundwater to channel exchange (due to the frequent overlap between floodplain cells and channel cells) instead of floodplain overflow (Bates et al. 2000; Kollet and Maxwell 2006).

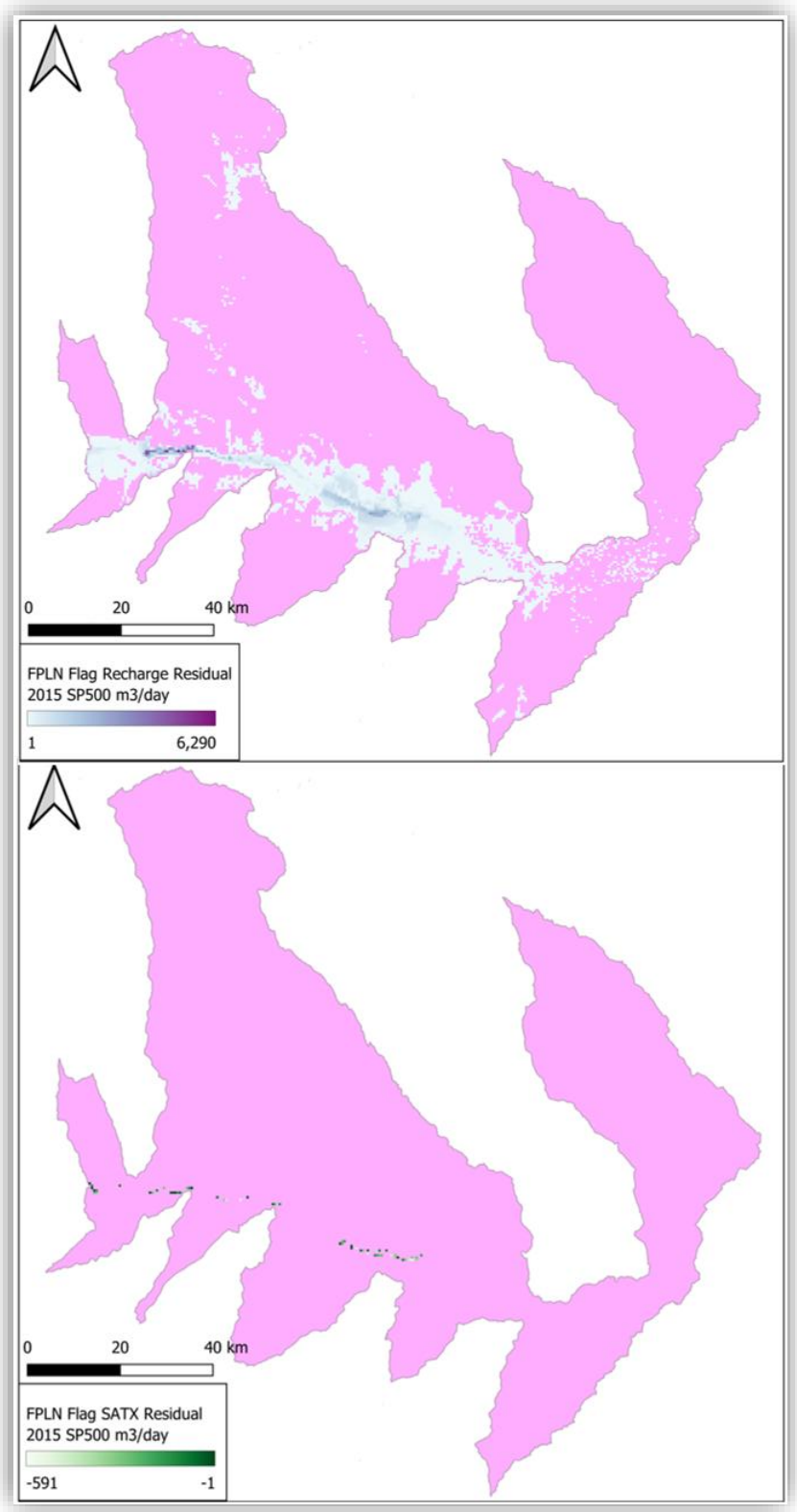

Figure 19: Discharge residuals from 2015 of the SP500 scenario with and without the floodplain flag for *gwflow* processes groundwater ET, recharge, and saturation excess flow.

3.4 Spatial and Temporal Analysis of Floodplain Processes

Floodplain processes were only active for a short duration. Figures 20-22 present daily groundwater balances for groups of cells representing the irrigated valley surrounding channel reaches (Figure 17) to analyze the spatial and temporal effects of floodplain exchange. Groups include cells that are not floodplain linked; fluxes are calculated from discharges across the entire group's area.

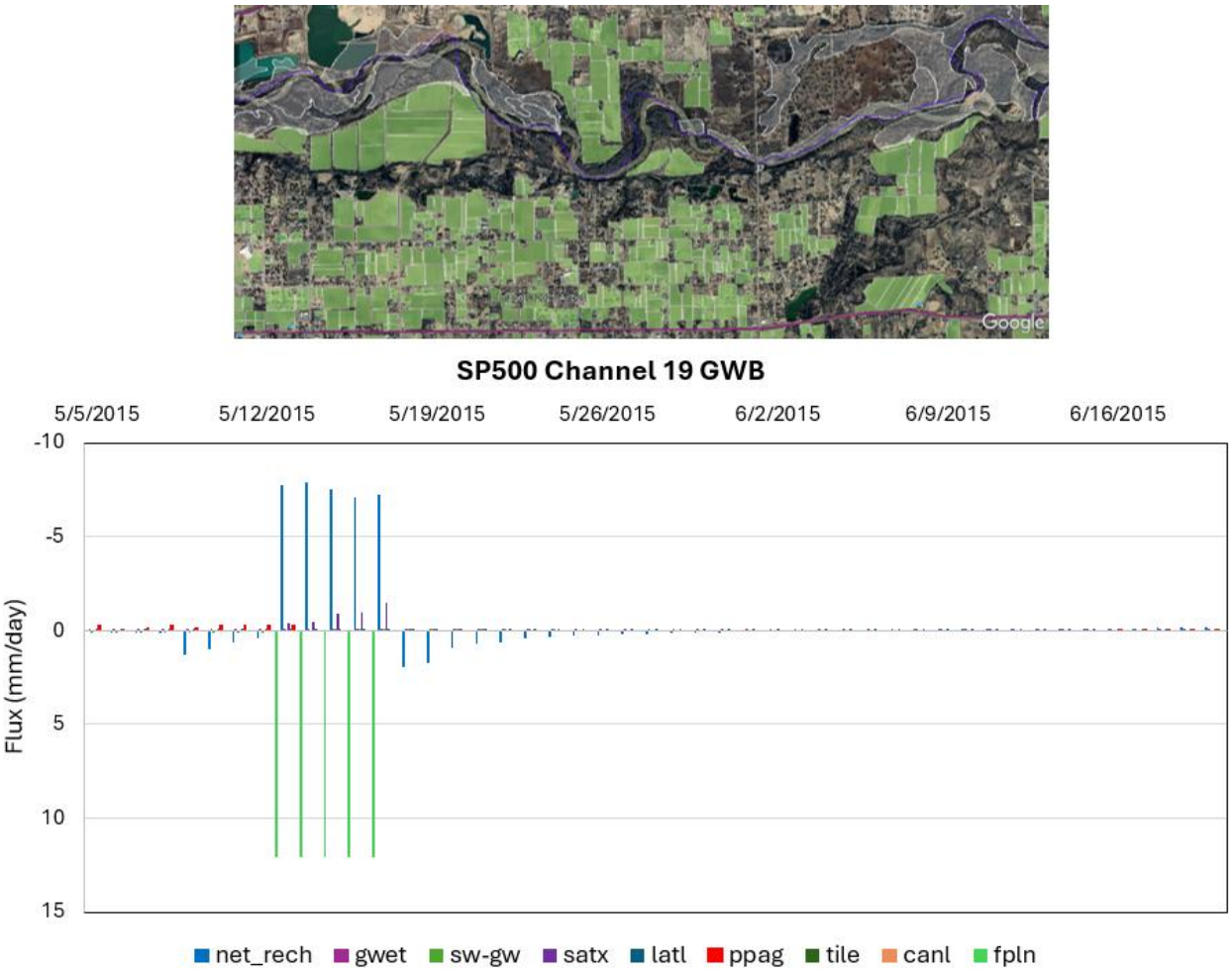

Figure 20: Daily group water balance surrounding the SP500 flood event for the group of cells representing the irrigated alluvial valley surrounding channel reach cha19. Floodplain landscapes are shaded white and irrigated fields are shaded green.

Channel 16 resides upstream of the confluence with the St Charles River. A near-zero net recharge is observed surrounding the lower water table higher in the watershed (Yimmer et al. 2023). At the front of rising streamflow, net recharge increased before exchange to the soil profile took over with rising water tables, followed by an immediate return to net positive recharge when flooding ended. Active floodplain exchange lasted five days with a constant flux of 12 mm/day, indicating flood stage and flooded area changed little across Group 19 cells. Groundwater evapotranspiration increased when overbank flow began, but reduced rapidly as flooding ended.

Above the confluence of the Huerfano River, the water balance group for Channel 16 showed a similar trend in groundwater process through the 500-year event. Groundwater pumping was turned off when flooding began, and did not resume until soil moisture and management schedule conditions resumed pumping 27 days later.

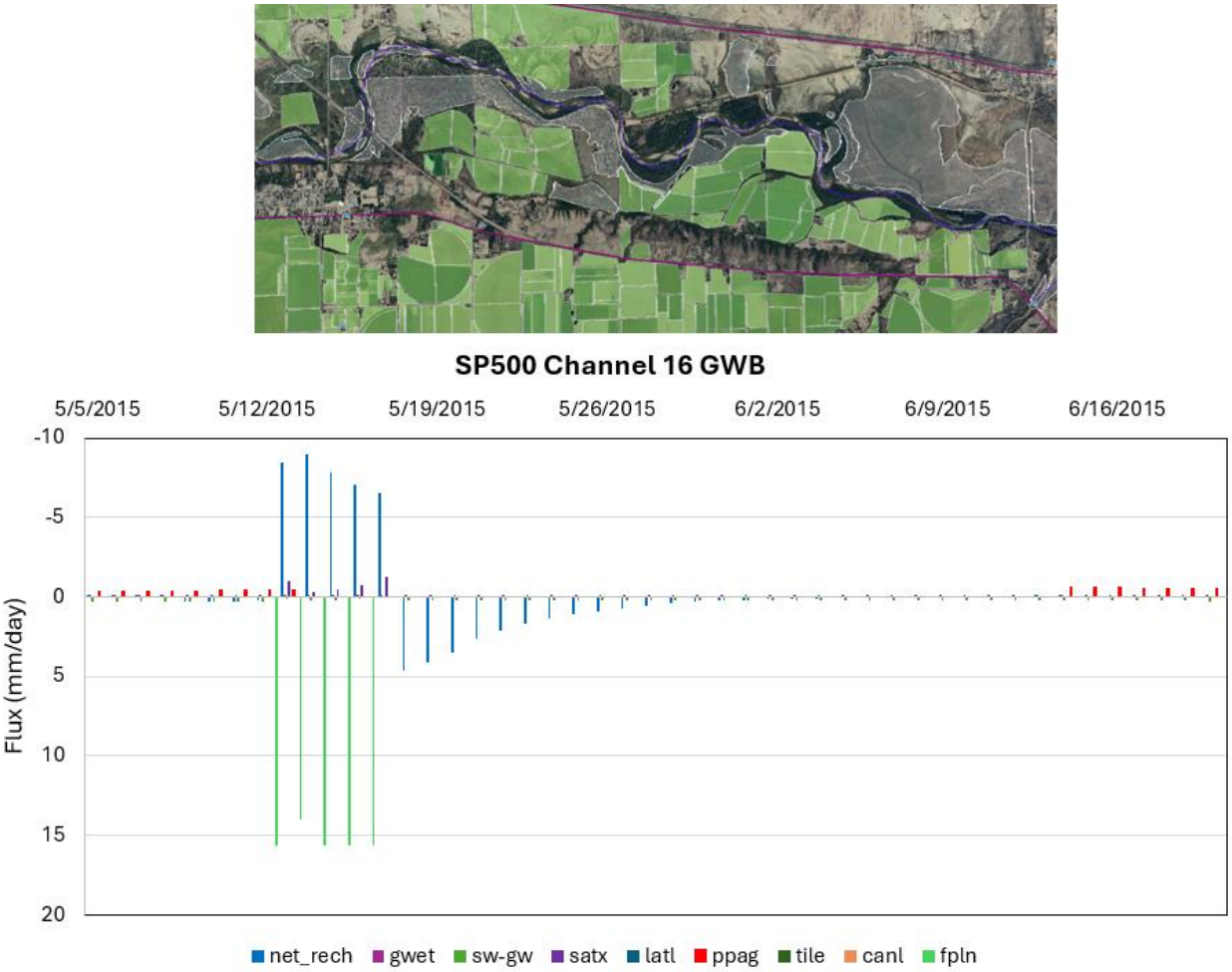

Figure 21: Daily group water balance surrounding the SP500 flood event for the group of cells representing the irrigated alluvial valley surrounding channel reach cha16 Floodplain landscapes are shaded white and irrigated fields are shaded green.

The Apishpa River enters the Arkansas River at the start of Channel 9, which is the furthest downstream channel reach with appreciable active floodplains (17 fpln cells). Active flooding occurred for an additional sixth day compared to upstream. Fluctuating amounts of saturation excess flows suggest the water table rose above the surface for a short duration at individual cells in different locations within the group.

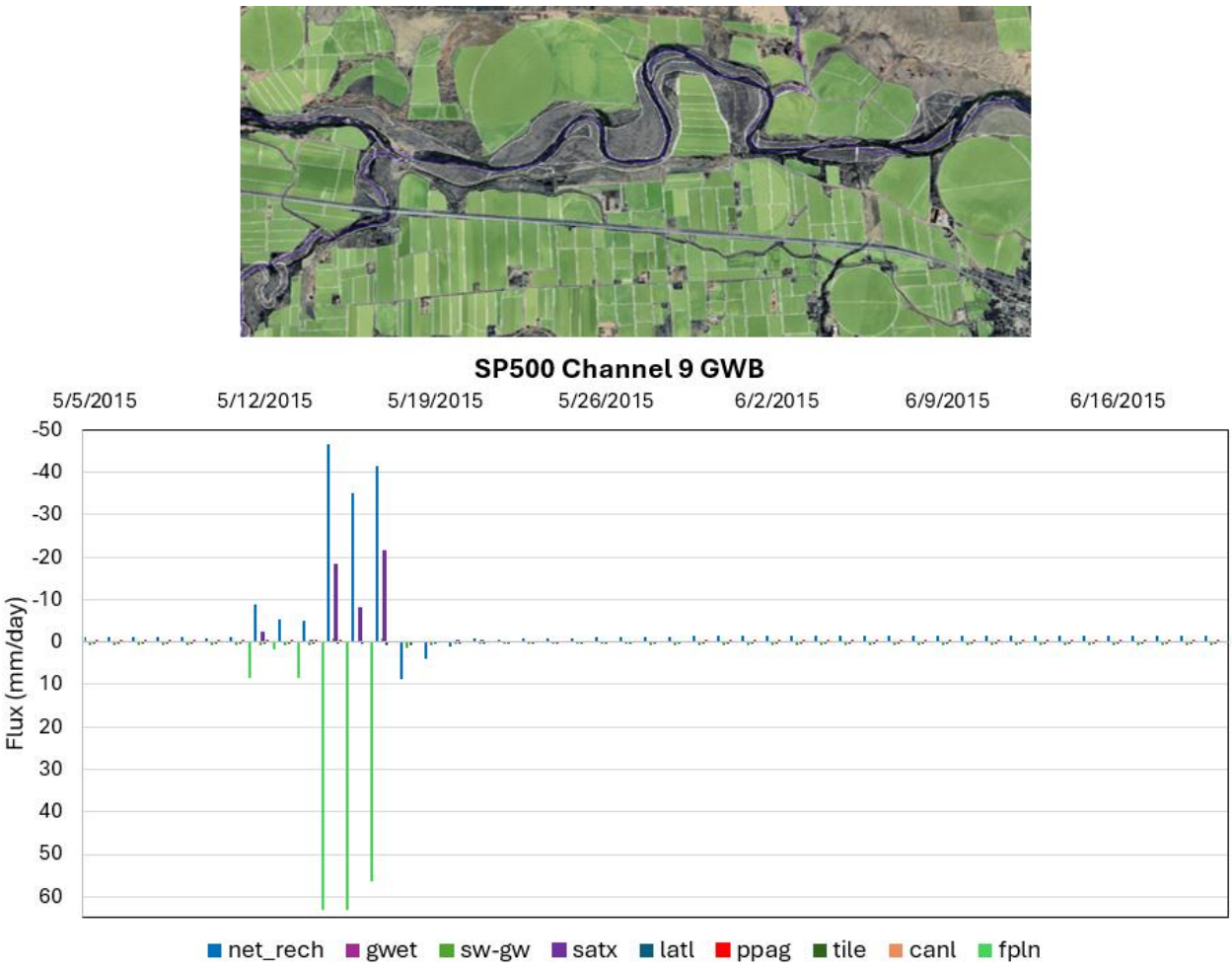

Figure 22: Daily group water balance surrounding the SP500 flood event for the group of cells representing the irrigated alluvial valley surrounding channel reach cha09. Floodplain landscapes are shaded white and irrigated fields are shaded green.

Floodplain exchange fluctuated within 10 mm/day in the first three days to exceed 60 mm/day in Group 9. Witnessed in Group 16 and Group 9 water balances, floodplain exchange decreased from day one to day two, then increased to day three following the first arrival of overbank flow. Local or upstream effects of attenuation and conveyance (Tull and Passalacqa 2025) may be apparent from inconsistent flood depths.

The Cross Section A-A' (Figure 23) transects a section of the LARV from North to South, briefly along Channel 9, and through four active floodplain cells (Figure 17). Most

hydrogeologic fluxes occur in the fluvial plain (Woessner 2000), with the highest floodplain discharges at cells with large areas of river beads (Schultz et al. 2024).

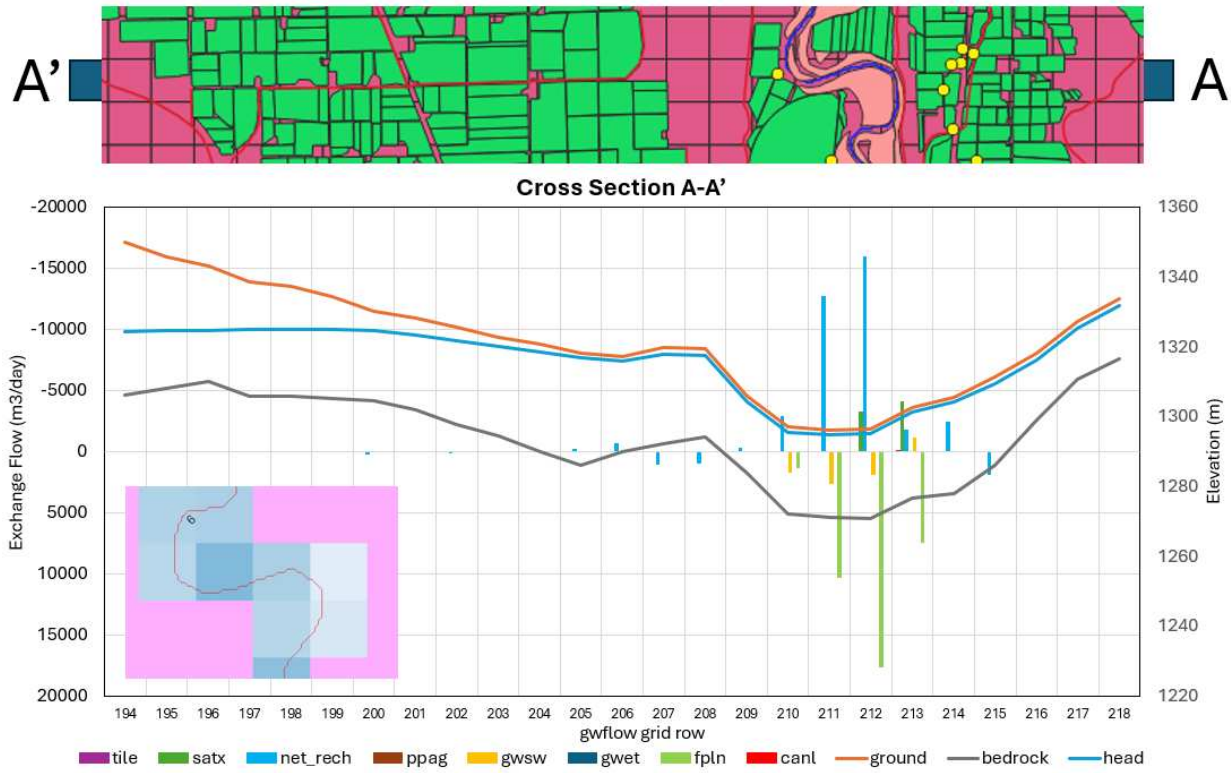

Figure 23: Cross section across the irrigated alluvial valley shows cell-by-cell groundwater exchanges and water table for May 2015 during the SP500 simulation. The inset figure represents floodplain exchange for individual cells.

4. SUMMARY AND CONCLUSIONS

4.1 Key Findings

Overbank flows occur very infrequently in the Lower Arkansas River Valley, but have potential to increase groundwater storage. This study involved creating a SWAT+ *gwflow* model that integrated floodplains Major groundwater balance components include 18 mm/year net exchange to the soil profile, 26 mm/year delivered to the aquifer from streams, and 13 mm/year withdrawals from pumping. Floodplain landscapes occupied 29 km^2 of the 8884 km^2 watershed, available for floodplain-aquifer processes. Active floodplain processes did not engage throughout the entire simulation period along the Arkansas river, but annual overbank flow in low-order streams contributes produces a small (<0.1%) annual contribution to groundwater storage . Groundwater storage increased by 2-4 % (2 mm/year) following a simulated 500-year streamflow event with 5 mm/yr flux gained through floodplains. Implementing floodplain landscapes and flood scenarios into this LARV SWAT+ *gwflow* models influences the hydrologic processes contributing to channelized flow and groundwater head beyond six months from inundation. Integrating floodplains for a 500-year event increases groundwater contributions to streamflow from 3% to 8%, reduces surface runoff, and increases saturation excess flow by over 600%.

Despite shallow water tables in the LARV, SWAT+ *gwflow* routines route discharges floodplain to aquifer; only unidirectional flows were observed from the floodplain adaption to darcy's law. Spatial resolution and floodplain delineation are very important when integrating floodplain processes to ensure inundation flagged by SWAT+ river routing triggers groundwater exchange.

Careful analysis of where and when cells activate groundwater exchange provides clues to where channel width and bank height promote overbank flow, conveyance of floodplain storage, and attenuation through the flood pulse.

4.2 Limitations and Future Work

A key challenge in assessing the impact of floodplain processes on general groundwater and stream hydrology is the lack of hydrologic data in floodplains, particularly during and immediately after a flooding event. This thesis relies on observed regional hydrologic responses (streamflow at river gages, groundwater head at monitoring wells) to calibrate and test the SWAT+ model. However, there is no direct response data within the floodplains to evaluate model performance during/after large flood events. Future work would require installation of monitoring wells in floodplains and instrumenting with data loggers, if results are assessed for the LARV, or finding watersheds with such data, if the goal is to verify SWAT+ floodplain algorithms.

Future work could focus on improving downstream streamflow predictions. Within the lower section of the watershed, streamflow projections did not fall within a satisfying range of observed flows and should be improved. Canal seepage was largely underestimated and can have implications for calculating groundwater head and groundwater return flows, which may affect groundwater storage in floodplain areas. Additional testing of initial head conditions and calibrating parameters such as canal hydraulic conductivities, specific storage, irrigation depths, and streambed hydraulic conductivity may reduce error from calibration targets. The addition of other considerable groundwater fluxes, like phreatophyte evapotranspiration and seepage from Lake Meredith may assist in reducing groundwater head error and effectively detail other processes.

For this thesis, floodplains were delineated using the spatial extent of riparian habitat, acquired from the U.S. Fish and Wildlife Service. However, there are alternative delineation methods for floodplains, such as GFPLAIN, a global high-resolution dataset of floodplains (Nardi et al., 2019). Appendix B shows the delineation of floodplains in the LARV using GFPLAIN. The effect of using this alternative delineation of floodplain extent could be compared with results from the current study, to address uncertainty in floodplain delineation.

This thesis does not explore the storage and transport of nutrients and other solutes within the stream-aquifer system of the LARV. Other studies have investigated the fate and transport of nitrate and selenium using a variety of surface-subsurface hydro-chemical models (Bailey et al., 2014; Shultz et al., 2018; Bailey et al., 2025). However, they did not include floodplain processes in their modeling approaches. Therefore, the effect of floodplain processes on the storage and transport of solutes between the aquifer and the river system has yet to be explored. This objective, however, is challenging due to the lack of solute data within the floodplain during and after flooding events. Further investigation of solute fate and transport through floodplains would enhance the applications of the *gwflow* process. A preliminary result of simulating nitrate fate and transport within the study region, under the influence of floodplains, is shown in Appendix C.

The implications of this research include water management, nutrient storage and river transport, and assessment of wetland development. Applying floodplain processes to other watersheds with more frequent flooding may promote alternative findings and should be investigated further.

FUNDING ACKNOWLEDGMENTS

Financial support for this study was provided by the Colorado Agricultural Experimental Station grant #COL00425.

5. REFERENCES

Abbas, Salam A., et al. "Estimation of groundwater storage loss using surface–subsurface hydrologic modeling in an irrigated agricultural region." *Scientific Reports* 15.1 (2025): 8350.

Abbas, S. A., Bailey, R. T., White, J. T., Arnold, J. G., White, M. J., Čerkasova, N., & Gao, J. (2024). A framework for parameter estimation, sensitivity analysis, and uncertainty analysis for holistic hydrologic modeling using SWAT+. *Hydrology and Earth System Sciences*, 28(1), 21-48.

Ajami, H., McCabe, M. F., & Evans, J. P. (2015). Impacts of model initialization on an integrated surface water–groundwater model. *Hydrological Processes*, 29(17), 3790-3801.

Almahawis, M. K., Bailey, R. T., Abbas, S. A., Arnold, J. G., & White, M. J. (2024). Investigating the impact of irrigation practices on hydrologic fluxes in a highly managed river basin. *Agricultural Water Management*, 301, 108954.

Arnold, J. G., Moriasi, D. N., Gassman, P. W., Abbaspour, K. C., White, M. J., Srinivasan, R., ... & Jha, M. K. (2012). SWAT: Model use, calibration, and validation. Transactions of the *ASABE*, 55(4), 1491-1508.

Baffaut, C., Baker, J. M., Biederman, J. A., Bosch, D. D., Brooks, E. S., Buda, A. R., Demaria, E. M., Elias, E. H., Flerchinger, G. N., Goodrich, D. C., Hamilton, S. K., Hardegree, S. P., Harmel, R. D., Hoover, D. L., King, K. W., Kleinman, P. J., Liebig, M. A., McCarty, G. W., Moglen, G. E., … Yasarer, L. M. W. (2020). Comparative analysis of water

budgets across the U.S. long-term agroecosystem research network. *Journal of Hydrology*, 588, 125021. https://doi.org/10.1016/j.jhydrol.2020.125021

Bailey, R. T., Bieger, K., Arnold, J. G., & Bosch, D. D. (2020). A New Physically-Based Spatially-Distributed Groundwater Flow Module for SWAT+. *Hydrology*, 7(4), Article 4. https://doi.org/10.3390/hydrology7040075

Bailey, R. T., Bieger, K., Flores, L., & Tomer, M. (2022). Evaluating the contribution of subsurface drainage to watershed water yield using SWAT+ with groundwater modeling. *Science of The Total Environment*, 802, 149962. https://doi.org/10.1016/j.scitotenv.2021.149962

Bailey, R. T., Abbas, S., Arnold, J., White, M., Gao, J., & Čerkasova, N. (2023). Augmenting the National agroecosystem model with physically based spatially distributed groundwater modeling. *Environmental Modelling & Software*, 160, 105589. https://doi.org/10.1016/j.envsoft.2022.105589

Bailey, R.T., Abbas, S., Arnold, J.G. and White, M.J., 2025. Assessing selenium fate and transport in a semi-arid river basin with and without human influence. *Water Research*, *277*, p.123335.

Bailey, R.T., Gates, T.K. and Ahmadi, M., 2014. Simulating reactive transport of selenium coupled with nitrogen in a regional-scale irrigated groundwater system. *Journal of Hydrology*, *515*, pp.29-46.

Bates, P. D., Stewart, M. D., Desitter, A., Anderson, M. G., Renaud, J. P., & Smith, J. A. (2000). Numerical simulation of floodplain hydrology. *Water Resources Research*, 36(9), 2517–2529. https://doi.org/10.1029/2000WR900102

Bedient, Philip B. and Wayne C. Huber. Hydrology and Floodplain Analysis. Prentice-Hall, Inc., Upper Saddle River, 2002.

Bieger, K., Arnold, J. G., Rathjens, H., White, M. J., Bosch, D. D., Allen, P. M., Volk, M., & Srinivasan, R. (2017). Introduction to SWAT+, A Completely Restructured Version of the Soil and Water Assessment Tool. *JAWRA Journal of the American Water Resources Association*, 53(1), 115–130. https://doi.org/10.1111/1752-1688.12482

Bieger, K., Arnold, J. G., Rathjens, H., White, M. J., Bosch, D. D., & Allen, P. M. (2019). Representing the Connectivity of Upland Areas to Floodplains and Streams in SWAT+. *JAWRA Journal of the American Water Resources Association*, 55(3), 578–590. https://doi.org/10.1111/1752-1688.12728

Busch, D. E., Ingraham, N. L., & Smith, S. D. (1992). Water uptake in woody riparian phreatophytes of the southwestern United States: a stable isotope study. *Ecological Applications*, 2(4), 450-459.

Calvi, C., Dapeña, C., Martinez, D. E., & Quiroz Londoño, O. M. (2018). Relationship between electrical conductivity, 18O of water and NO3 content in different streamflow stages. *Environmental Earth Sciences*, 77(6), 248.

Cartwright, I., Werner, A. D., & Woods, J. A. (2019). Using geochemistry to discern the patterns and timescales of groundwater recharge and mixing on floodplains in semi-arid regions. *Journal of Hydrology*, 570, 612–622. https://doi.org/10.1016/j.jhydrol.2019.01.023

Dewitz, J. (2021). National land cover database (NLCD) 2019 products. US Geological Survey, 10, P9KZCM54.

Doherty, J. (2010). PEST User-Manual: Model-independent parameter estimation. Watermark Numerical Computing.

Gates, T. K., Garcia, L. A., and Labadie, J. W. (2006).“Toward optimal water management in Colorado’s Lower Arkansas River Valley: monitoring and modeling to enhance agriculture and environment.” Colorado Water Resour. Res. Inst. Completion Report No. 205, Colorado Agric. Exp. Station Tech. Report TR06-10, Colorado State University, Fort Collins, CO.

Gates, T. K., Garcia, L. A., Hemphill, R. A., Morway, E. D., & Elhaddad, A. (2012). Irrigation practices, water consumption, & return flows in Colorado's Lower Arkansas River Valley: field and model investigations.

Gesch, D. B., Evans, G. A., Oimoen, M. J., & Arundel, S. (2018). The National Elevation Dataset. U.S. Geological Survey.

Harvey, J. W., & Wagner, B. J. (2000). Quantifying hydrologic interactions between streams and their subsurface hyporheic zones. *Streams and ground waters*, 3-44.

Horton, J. D. (2017). The state geologic map compilation (SGMC) geodatabase of the conterminous United States: US geological survey data release. US Geological Survey.

Jolly, I. D., & Rassam, D. W. (2009, July). A review of modelling of groundwater-surface water interactions in arid/semi-arid floodplains. In 18th World IMACS/MODSIM Congress, Cairns, Australia (pp. 3088-3094).

Junk, W. J., Bayley, P. B., & Sparks, R. E. (1989). The flood pulse concept in river-floodplain systems. Canadian Special Publications Fisheries and Aquatic Sciences, 106, 110–127.

Kendy, E., & Bredehoeft, J. D. (2006). Transient effects of groundwater pumping and surface-water irrigation returns on streamflow. *Water Resources Research*, 42(8). https://doi.org/10.1029/2005WR004792

Knox, R. L., Morrison, R. R., & Wohl, E. E. (2022). Identification of Artificial Levees in the Contiguous United States. *Water Resources Research*, 58(4), e2021WR031308. https://doi.org/10.1029/2021WR031308

Kollet, S. J., & Maxwell, R. M. (2006). Integrated surface–groundwater flow modeling: A free-surface overland flow boundary condition in a parallel groundwater flow model. *Advances in Water Resources*, 29(7), 945-958.

Maier, N., Breuer, L., & Kraft, P. (2017). Prediction and uncertainty analysis of a parsimonious floodplain surface water-groundwater interaction model. *Water Resources Research*, 53(9), 7678–7695. https://doi.org/10.1002/2017WR020749

McCuen, R. H., Knight, Z., & Cutter, A. G. (2006). Evaluation of the Nash–Sutcliffe efficiency index. *Journal of Hydrologic Engineering*, 11(6), 597-602.

Molina-Navarro, E., Nielsen, A., & Trolle, D. (2018). A QGIS plugin to tailor SWAT watershed delineations to lake and reservoir waterbodies. *Environmental Modelling & Software*, *108*, 67-71.

Morway, E. D., Gates, T. K., & Niswonger, R. G. (2013). Appraising options to reduce shallow groundwater tables and enhance flow conditions over regional scales in an irrigated alluvial aquifer system. *Journal of Hydrology*, *495*, 216-237.

Nardi, F., Annis, A., Di Baldassarre, G., Vivoni, E. R., & Grimaldi, S. (2019). GFPLAIN250m, a global high-resolution dataset of Earth's floodplains. Scientific Data, 6(1), Article 1. https://doi.org/10.1038/sdata.2018.309

Navas, R., Gelós, M., & Bailey, R. (2025). Quantifying Baseflow Changes Due to Irrigation Expansion Using SWAT+ *gwflow*. *Water*, 17(11), 1680.

Niemann, J. D., Lehman, B.M., Gates, T.K., Hallberg, N.O., and Elhaddad, A. (2011). "Impact of shallow groundwater on evapotranspiration losses from uncultivated land in an irrigated river valley." *Journal of Irrigation and Drainage Engineering*, 137(8): 501-512

Opperman, J. J., Luster, R., McKenney, B. A., Roberts, M., & Meadows, A. W. (2010). Ecologically Functional Floodplains: Connectivity, Flow Regime, and Scale. *JAWRA Journal of the American Water Resources Association*, 46(2), 211–226. https://doi.org/10.1111/j.1752-1688.2010.00426.x

Reitz, M., Sanford, W. E., Senay, G. B., & Cazenas, J. (2017). Annual estimates of recharge, quick-flow runoff, and evapotranspiration for the contiguous US using empirical regression equations. *JAWRA Journal of the American Water Resources Association*, 53(4), 961-983.

Saksena, S., & Merwade, V. (2017). Integrated Modeling of Surface-Subsurface Processes to Understand River-Floodplain Hydrodynamics in the Upper Wabash River Basin. 60–68. https://doi.org/10.1061/9780784480595.006

Shangguan, W., Hengl, T., Mendes de Jesus, J., Yuan, H., & Dai, Y. (2017). Mapping the global depth to bedrock for land surface modeling. *Journal of Advances in Modeling Earth Systems*, 9(1), 65–88. https://doi.org/10.1002/2016MS000686

Schulz, E.Y., Morrison, R.R., Bailey, R.T., Raffae, M., Arnold, J.G. and White, M.J., 2024. River corridor beads are important areas of floodplain-groundwater exchange within the Colorado River headwaters watershed. *Hydrological Processes*, *38*(9), p.e15282.

Shultz, C.D., Gates, T.K. and Bailey, R.T., 2018. Evaluating best management practices to lower selenium and nitrate in groundwater and streams in an irrigated river valley using a calibrated fate and reactive transport model. *Journal of hydrology*, *566*, pp.299-312.

Shangguan, W., Hengl, T., Mendes de Jesus, J., Yuan, H., & Dai, Y. (2017). Mapping the global depth to bedrock for land surface modeling. *Journal of Advances in Modeling Earth Systems*, 9(1), 65-88.

Soil Survey Staff, Natural Resources Conservation Service, United States Department of Agriculture. Soil Survey Geographic (SSURGO) Database. Available online. Accessed November 1, 2023.

Susfalk, R., Sada, D., Martin, C., Young, M., Gates, T., Rosamond, C., Mihevc, T., Arrowood, T., Shanafield, M., Epstein, B., Fizgerald, B., Lutz, A., Woodrow, J., Miller,G., and Smith, D. (2008). "Evaluation of linear anionic polyacrylamide (LA-PAM) application to water delivery canals for seepage reduction." DHS Pub. No. 41245, Desert Research Institute, Reno, NV.

Triana, E., Labadie, J. W., and Gates, T. K. (2010a). "River GeoDSS for agro-environmental enhancement of Colorado's Lower Arkansas River Basin. I: Model development and calibration." *Journal of Water Resources Planning and Management*.

Tull, N., & Passalacqua, P. (2025). Floodwave attenuation as a function of floodplain storage, secondary channel conveyance, and discharge. *Water Resources Research*, 61,e2024WR038582. https://doi.org/10.1029/2024WR038582

U.S. Department of Agriculture, National Agricultural Statistics Service. (2019). 2017 Census of Agriculture: County Profile – Otero County, Colorado (Report No. CP-08089). USDA National Agricultural Statistics Service. https://www.nass.usda.gov/Publications/AgCensus/2017/Online_Resources/County_Profiles/Colorado/cp08089.pdf

Valayamkunnath, P., Barlage, M., Chen, F., Gochis, D. J., & Franz, K. J. (2020). Mapping of 30-meter resolution tile-drained croplands using a geospatial modeling approach. *Scientific Data*, 7(1), 257.

Wagner, P. D., Bieger, K., Arnold, J. G., & Fohrer, N. (2022). Representation of hydrological processes in a rural lowland catchment in Northern Germany using SWAT and SWAT+. *Hydrological Processes*, 36(5), e14589.

Wasko, C., & Nathan, R. (2019). Influence of changes in rainfall and soil moisture on trends in flooding. *Journal of Hydrology*, 575, 432-441.

White, M. J., Arnold, J. G., Bieger, K., Allen, P. M., Gao, J., Čerkasova, N., Gambone, M., Park, S., Bosch, D. D., Yen, H., & Osorio, J. M. (2022). Development of a Field Scale SWAT+ Modeling Framework for the Contiguous U.S. *JAWRA Journal of the American Water Resources Association*, n/a(n/a). https://doi.org/10.1111/1752-1688.13056

Wohl, E. (2021). An Integrative Conceptualization of Floodplain Storage. Reviews of *Geophysics*, 59(2). https://doi.org/10.1029/2020RG000724

Woessner, W. W. (2000). Stream and Fluvial Plain Ground Water Interactions: Rescaling Hydrogeologic Thought. *Groundwater*, 38(3), 423–429. https://doi.org/10.1111/j.1745-6584.2000.tb00228.x

Yimer, E. A., Bailey, R. T., Piepers, L. L., Nossent, J., & Van Griensven, A. (2023). Improved representation of groundwater–surface water interactions using SWAT+ *gwflow* and modifications to the *gwflow* module. *Water*, 15(18), 3249.

Zhou, Y., & Li, W. (2011). A review of regional groundwater flow modeling. *Geoscience Frontiers*, 2(2), 205-214.

APPENDIX A: Calibrated Parameter Descriptions

Additional information on parameters used in sensitivity analysis and calibration is provided in this section. Reference parameters listed below with values in Table 2.

cntable.lum

Curve numbers a-d for the three most prevalent SWAT+ landcover types (rcstrog, brush_f, pastg).

hydrology.hyd

Soil evaporation consumption factor (esco), the plant evaporation consumption factor (epco), and the percolation coefficient (perco).

gwflow.input

Recharge delay (rech_del), hydraulic conductivity (kaquifer) specific yield (syaquif_), and streambed hydraulic conductivity (bed_k) for each of the geologic zones characterized by the USGS used in this model. In addition, streambed thickness (bed_thick) and streambed depth below the surface (bed_depth).

gwflow.tile

Tile drainage depth (tile_depth), tile drain surface area (tile_area), and tile drain hydraulic conductivity.

gwflow.floodplain

Floodplain hydraulic conductivities (kfloodplain) for each geologic zone with floodplain landscapes.

gwflow.canal

Canal hydraulic conductivity for each individual canal (canal_k_).

parameters.bsn

Surface runoff coefficient.

hyd-sed-lte.cha

Channel hydraulic conductivity (k_mainstem) and manning's n for the Arkansas River (manningmst).

snow.sno

Temperature lag to initiate snowmelt (temp_lag_), maximum snowfall temperature (melt_max_), and temperature to initiate snow melting (melt_temp_).

topography.hyd

Erosion slope lengths.

soils.sol

Available water contents for soil types most prevalent in floodplains.

APPENDIX B: Alternative Floodplain Delineation

Additional analysis was performed using continuous floodplain landscapes delineated by the GFPLAIN algorithm (Nardi et al., 2019), which defines floodplain landscapes from DEM values. Model output (Figure B.1) shows a much wider swath of activated floodplain cell in upstream regions as compared to the method of using riparian habitat to delineate floodplain extent, but floodplains did not activate downstream near Catlin Dam along Channel 9. Inactive cells flagged as floodplains with the "riparian" delineation during this in this study also became active with GFPLAIN. Further investigation is needed as SWAT+ routines should spatially initiate overbank flow with different floodplain delineations.

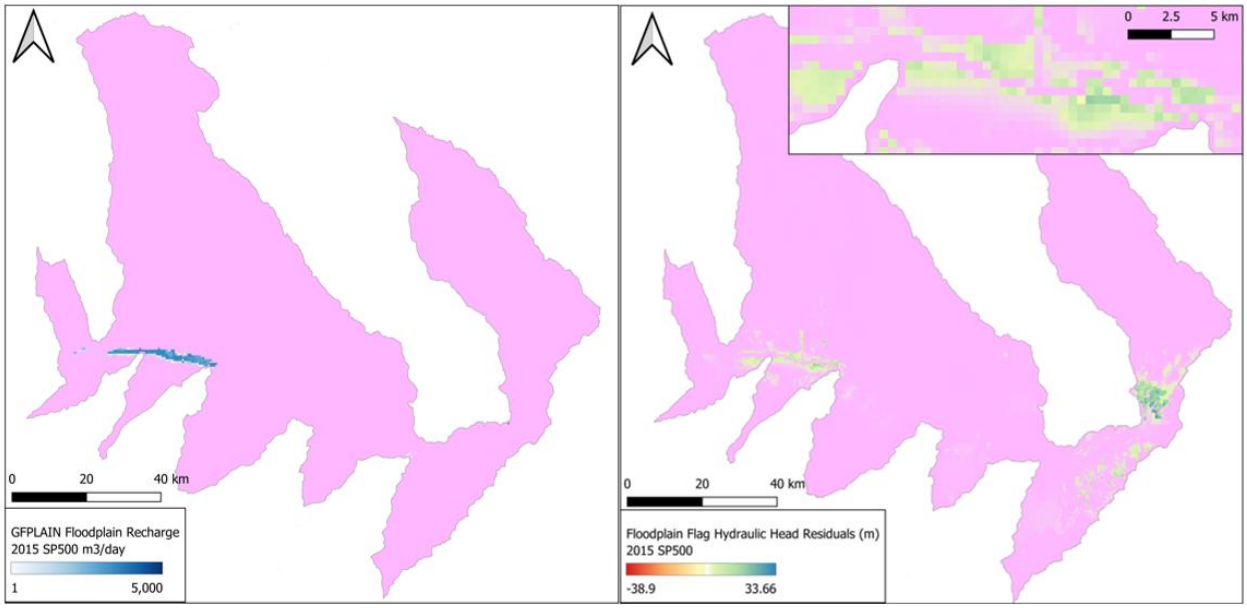

Figure B.1: Map on left shows 2015 SP500 floodplain recharge when floodplains are delineated with GFPLAIN. Map to the right shows hydraulic head residuals modeling with and without the floodplain flag using GFPLAIN during the flood scenario.

The high head residuals East of Horse Creek are from an activated cell on along a low-order stream that simulates excessive floodplain exchange.

APPENDIX C: Nitrogen Modeling

Solute data was added to the model for additional analysis. Nitrate, nitrite, and ammonium concentrations from surface waters were obtained from the Water Quality Portal (https://waterqualitydata.us) for each Inlet. Point source files require continuous daily values for all attributes of interest, however, infrequent sampling at many inlets left many gaps in the model testing time series. Plotting specific conductance to constituent concentrations (Calvi et al. 2015) did not show correlation at any inlets where specific conductance data were available. To proceed, the median concentrations measured from streams were applied as a constant concentration to calculate daily loads of each constituent. Initial groundwater concentrations of nitrate were tested with the default value of 3 g/m^3 N/NO_3, then reset with model output groundwater concentrations from the end of the 1992-2020 simulation.

Table 7: Median concentrations of nitrogen constituents used for model input.

	Median concentrations (mg/L)						
	Pueblo Dam	Fountain Creek	St Charles River	Huerfano River	Apishpa River	Timpas Creek	Horse Creek
NO3	0.150	1.44	0.150	0.150	1.64	2.00	1.64
NH4	0.100	0.015	0.007	0.007	0.012	0.020	0.012
NO2	0.010	0.038	0.030	0.030	0.010	0.068	0.010

The distribution of nitrate concentrations in groundwater across the watershed is mapped in Figure C.1. Transient simulation removed nitrate from many upland regions, and the distribution looks similar to the map of recharge from deep percolation. Concentrations vary in the range of 1 to 30 mg/L in irrigated areas, with several cells at the far reaches of the Colorado Canal exceeding 60 mg/L.

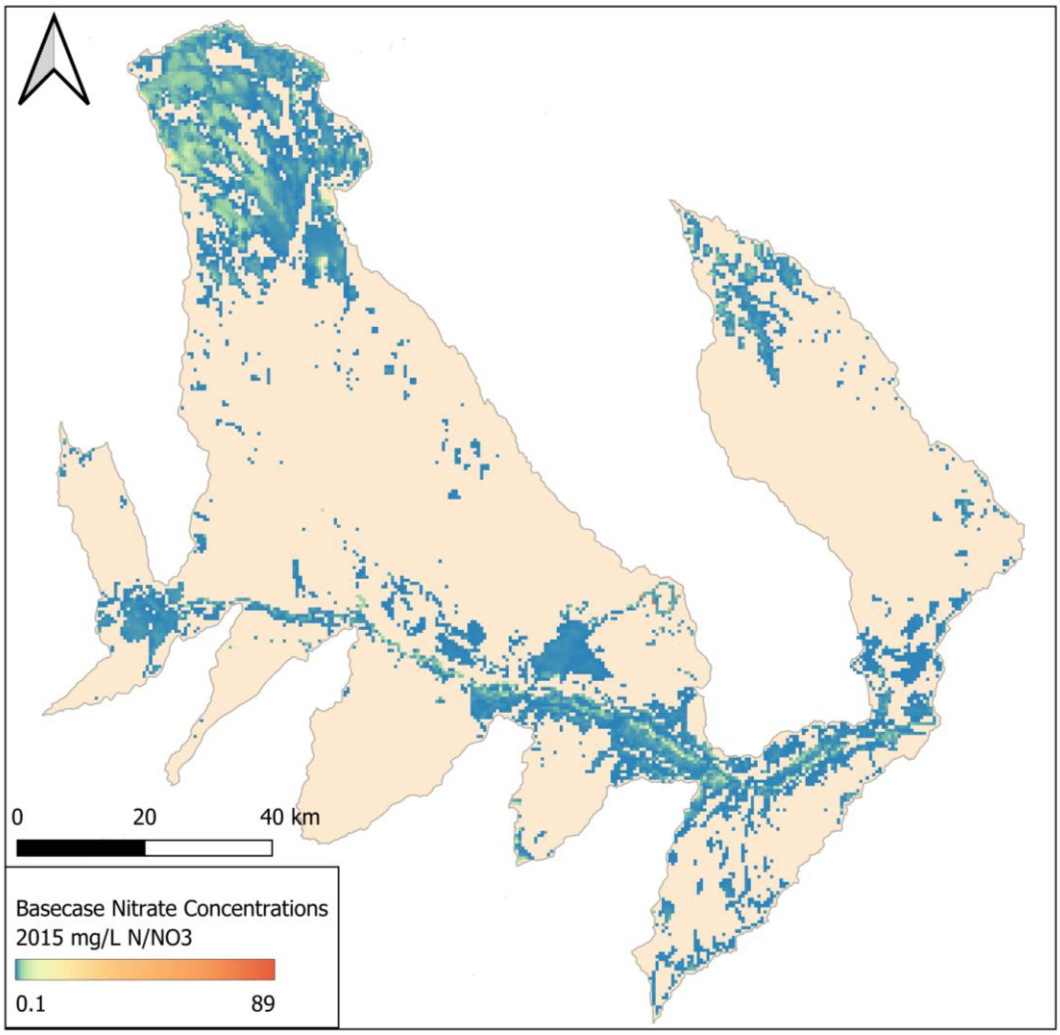

Figure C.1: Modeled nitrate concentrations in groundwater for the year 2015.

An in-depth analysis of nitrogen fate and transport was not performed, but SP500 scenarios results show that floodplain processes contribute to nitrate loading and affect concentrations in groundwater (Figure C.2).

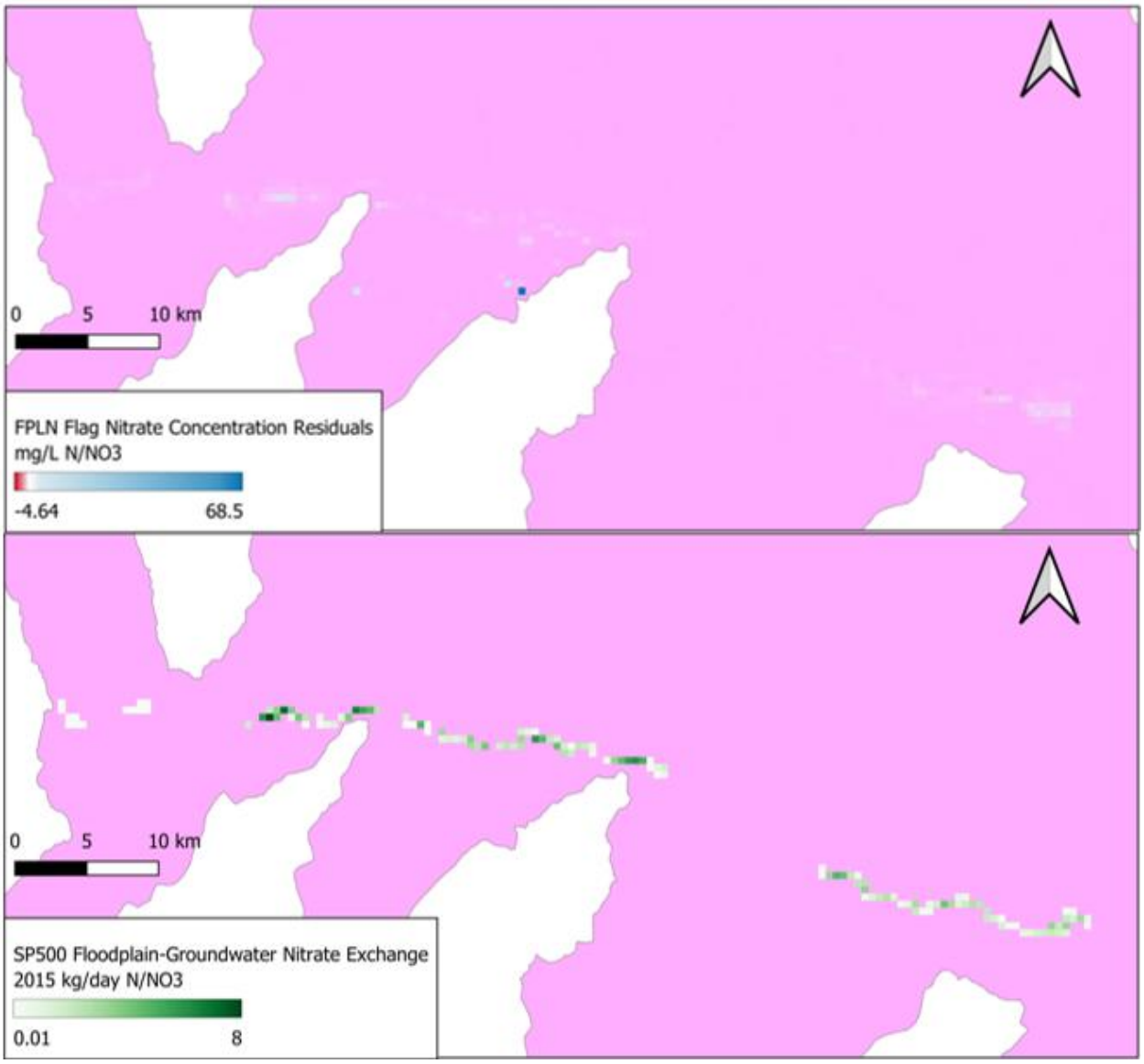

Figure C.2: Top map shows groundwater nitrate concentration residuals during the SP500 scenario from modeling with and without the floodplain flag. Bottom map includes simulated masses of nitrate loading through floodplains during 2015 of the SP500 scenario.